The assembly, regulation and function of the mitochondrial respiratory chain

Irene Vercellino and Leonid A. Sazanov ✉

Abstract | The mitochondrial oxidative phosphorylation system is central to cellular metabolism. It comprises five enzymatic complexes and two mobile electron carriers that work in a mitochondrial respiratory chain. By coupling the oxidation of reducing equivalents coming into mitochondria to the generation and subsequent dissipation of a proton gradient across the inner mitochondrial membrane, this electron transport chain drives the production of ATP, which is then used as a primary energy carrier in virtually all cellular processes. Minimal perturbations of the respiratory chain activity are linked to diseases; therefore, it is necessary to understand how these complexes are assembled and regulated and how they function. In this Review, we outline the latest assembly models for each individual complex, and we also highlight the recent discoveries indicating that the formation of larger assemblies, known as respiratory supercomplexes, originates from the association of the intermediates of individual complexes. We then discuss how recent cryo-electron microscopy structures have been key to answering open questions on the function of the electron transport chain in mitochondrial respiration and how supercomplexes and other factors, including metabolites, can regulate the activity of the single complexes. When relevant, we discuss how these mechanisms contribute to physiology and outline their deregulation in human diseases.

Reducing equivalents
Chemical species that transfer the equivalent of one electron in redox reactions.

Quinol
Reduced form of quinone. In the context of the electron transport chain, it is produced by complexes I, II and III_2 and utilized by complex III_2.

ATP synthase
An enzyme that catalyses the formation of ATP using ADP and inorganic phosphate. Various types of ATPases exist in nature, including A-ATPases ('A' stands for 'archaeal'), F-ATPases ('F' stands for '(phosphorylation) factor') and V-ATPases ('V' stands for 'vacuolar'). The mammalian ATP synthase is an F-type ATPase.

Institute of Science and Technology Austria, Klosterneuburg, Austria.
✉*e-mail: sazanov@ist.ac.at*

https://doi.org/10.1038/s41580-021-00415-0

Mitochondrial oxidative phosphorylation (OXPHOS) is a key mechanism of energy production in eukaryotic cells[1]. Its machinery comprises four inner mitochondrial membrane (IMM)-embedded protein complexes — complex I (also referred to here as CI) or NADH:ubiquinone oxidoreductase, complex II (also referred to here as CII) or succinate dehydrogenase (SDH), dimeric complex III_2 (also referred to here as $CIII_2$) or cytochrome bc_1 oxidoreductase, and complex IV (also referred to here as CIV) or cytochrome *c* oxidase — and two mobile electron carriers — the membrane-embedded hydrophobic ubiquinone and the soluble cytochrome *c*[2] — that together are referred to as electron transport chain (ETC) (FIG. 1a). The activity of the ETC controls a plethora of physiological processes and as such is subject to various levels of regulation (FIG. 1b).

Functionally, the ETC components utilize the energy from nutritive substances in the form of the reducing equivalents in NADH and succinate, coming mainly from the Krebs cycle[3] (FIG. 1a), to generate an electrochemical proton gradient across the IMM. The oxidation of the reducing equivalents by the ETC leads to the reduction of molecular oxygen to water and is coupled to the pumping of protons across the IMM. Three of the ETC complexes — complexes I, III_2 and IV — show proton-pumping activity, for which they use three different mechanisms; namely, transfer across antiporter subunits (complex I)[4], the Q cycle (complex III_2)[5,6] and a still debated water-gated mechanism (complex IV)[7] (FIG. 2a). Complex II does not pump protons, but it contributes to the reduction of ubiquinone[8], which serves as an electron source for complex III_2. Complex III_2 accepts electrons in the form of quinol from both complex I and complex II, which in turn oxidize NADH and succinate, respectively, as well as from several dehydrogenases (dihydroorotate dehydrogenase, electron transfer flavoprotein:ubiquinone oxidoreductase, glycerol 3-phosphate dehydrogenase, choline dehydrogenase, proline dehydrogenase, sulfide:quinone oxidoreductase) also reducing ubiquinone[9,10]. Complex III_2 then reduces cytochrome *c*, which in turn shuttles to complex IV and donates its electron for the final reduction of oxygen. The generated proton gradient is then exploited by the fifth component of the system, ATP synthase, which phosphorylates ADP to ATP, the universal energy currency of cells[11].

The components of the OXPHOS chain are multiprotein complexes that need to be assembled in the IMM from subunits encoded both in the nuclear DNA and in the mitochondrial DNA[12,13] (information summarized in TABLE 1) and need to be equipped with several different cofactors[14], such as iron–sulfur clusters (Fe–S clusters)[15] and haem groups[16] (FIG. 2b,c). The protein components can also be divided into core subunits, which are required

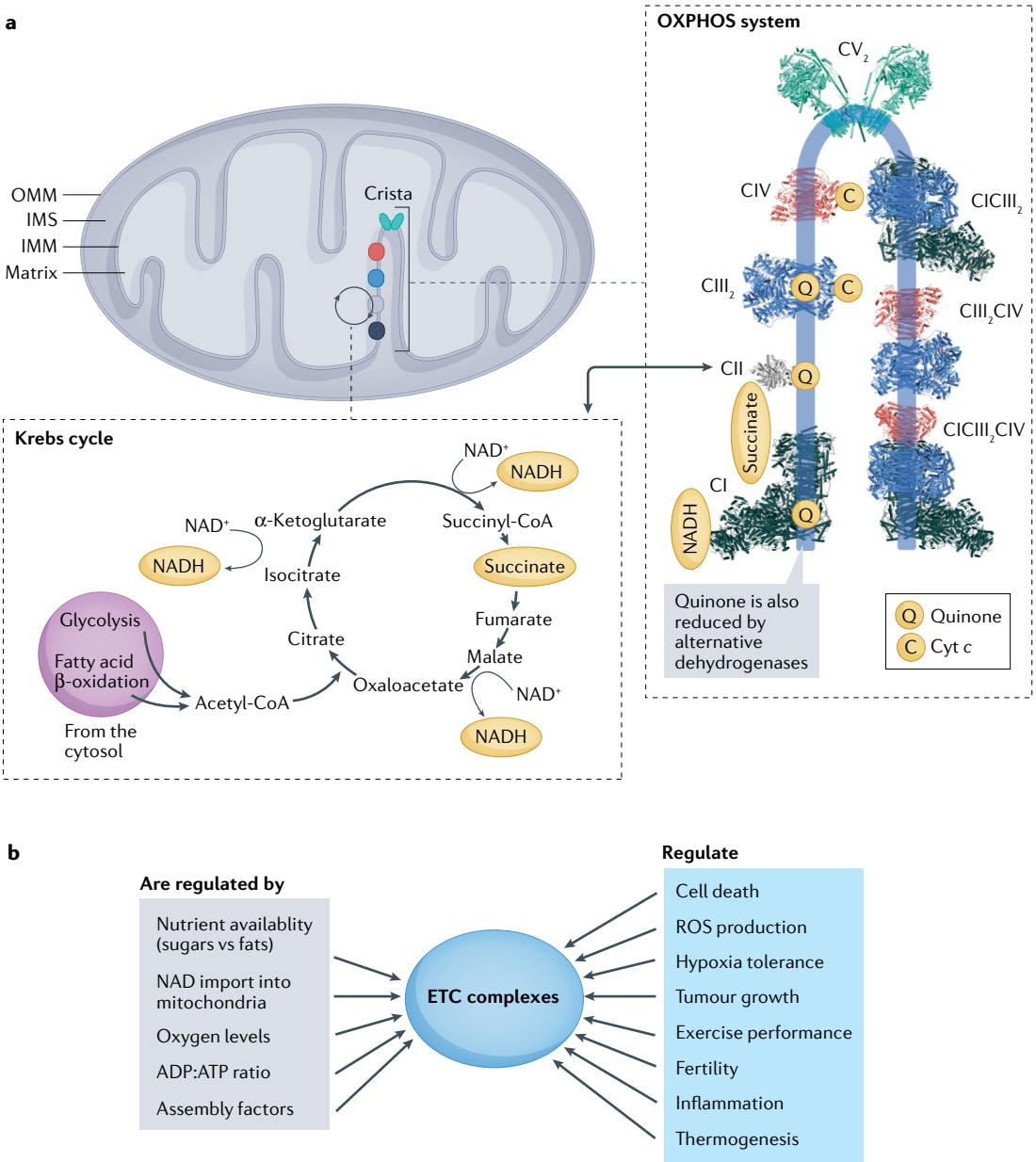

Fig. 1 | **Overview of the structure and function of the mitochondrial oxidative phosphorylation machinery.** **a** | A mitochondrion, with the oxidative phosphorylation (OXPHOS) complexes and their interactions/regulations within and outside mitochondria indicated. The double arrow emphasizes that complex II (CII) belongs to both the Krebs cycle and the OXPHOS system. The electron carriers NADH, succinate, quinone (Q) and cytochrome *c* (C) are depicted as yellow ovals. NADH donates electrons to complex I (CI) and succinate donates electrons to complex II (CII), while quinone shuttles electrons from complexes I and II to complex III_2 ($CIII_2$) and cytochrome *c* (cyt *c*) shuttles electrons from complex III_2 to complex IV (CIV). The inset on the right depicts a zoom in on a mitochondrial crista. The OXPHOS components shown as shapes in the scheme on the left are shown as models in matching colours, together with their higher-order organization into supercomplexes: complex I (Protein Data Bank (PDB) ID 6ZKC) is coloured dark slate grey, complex II (PDB ID 1ZOY) is light grey, complex III_2 (PDB ID 6Q9E) is blue, complex IV (PDB ID 5IY5) is salmon, supercomplexes $CICIII_2CIV$ (PDB ID 5J4Z), $CICIII_2$ (PDB ID 6QBX) and $CIII_2CIV$ (PDB ID 7O3C) are coloured according to the individual complexes and ATP synthase dimer (CV_2; PDB ID 7AJF) is cyan. ATP synthase is found at the cristae edges, where its dimers bend and shape the membrane. Complexes I, II, III_2 and IV and their supercomplexes are found in the flat areas of cristae. **b** | Overview of the factors that regulate the electron transport chain (ETC) function (on the left) and of the processes regulated by the ETC (right), as discussed throughout the text. IMM, inner mitochondrial membrane; IMS, intermembrane space; OMM, outer mitochondrial membrane; ROS, reactive oxygen species.

Iron–sulfur clusters
(Fe–S clusters). Groups of iron and sulfur atoms coordinated to protein residues acting as cofactors in redox reactions due to the ability to transfer electrons from or to other Fe–S clusters or different types of donors/acceptors while undergoing oxidation and reduction cycles. The xFe–yS nomenclature refers to the number of Fe (x) and S (y) atoms in the cluster.

Haem groups
Redox cofactors featuring an iron atom at the centre of a porphyrin structure. The iron atom can undergo cycles of oxidoreduction, thereby transferring electrons from the donor to acceptors along the electron transport chain. There are three types of haems in the electron transport chain, characterized by different substituents on the porphyrin ring: haems *a* (*a* and a_3) of complex IV, haems *b* (b_H and b_L) of complex III_2, haem *c* of cytochrome *c* and haem c_1 of complex III_2.

for activity and are conserved across all the domains of life, and supernumerary subunits, which are usually not present in simpler organisms such as bacteria and whose function has been ascribed to the assembly and stability of the complexes that are likely required in organisms with more complex metabolism[17–19] (FIG. 2d). Given the complexity of the ETC structure and the dual origin of the subunits, it is not surprising that a plethora of

assembly factors are involved in the process, with various functions such as regulation of transcription and translation, post-translational modifications, association with cofactors, insertion in the membrane, proteolysis and clearance of fragments and stabilization of assembly intermediates. For some factors their specific role is yet to be determined. Interestingly, as shown in TABLE 1, complex IV has the highest number of associated assembly factors (almost 50), despite having a similar number of unique subunits as complex III_2. Complex I biogenesis is also aided by a significant number of assembly factors (around 20), but this is justified by its size (1 MDa) and the presence of several different cofactors (that is, flavin mononucleotide and the Fe–S clusters). Conversely, complexes III_2 and V, despite their size (around 0.5 MDa, which is larger than complex IV), have been linked to fewer than ten assembly factors each. Finally, four factors have been found to assist the assembly of complex II, the smallest complex of the chain (120 kDa), composed of only four subunits. Importantly, several mitochondrial

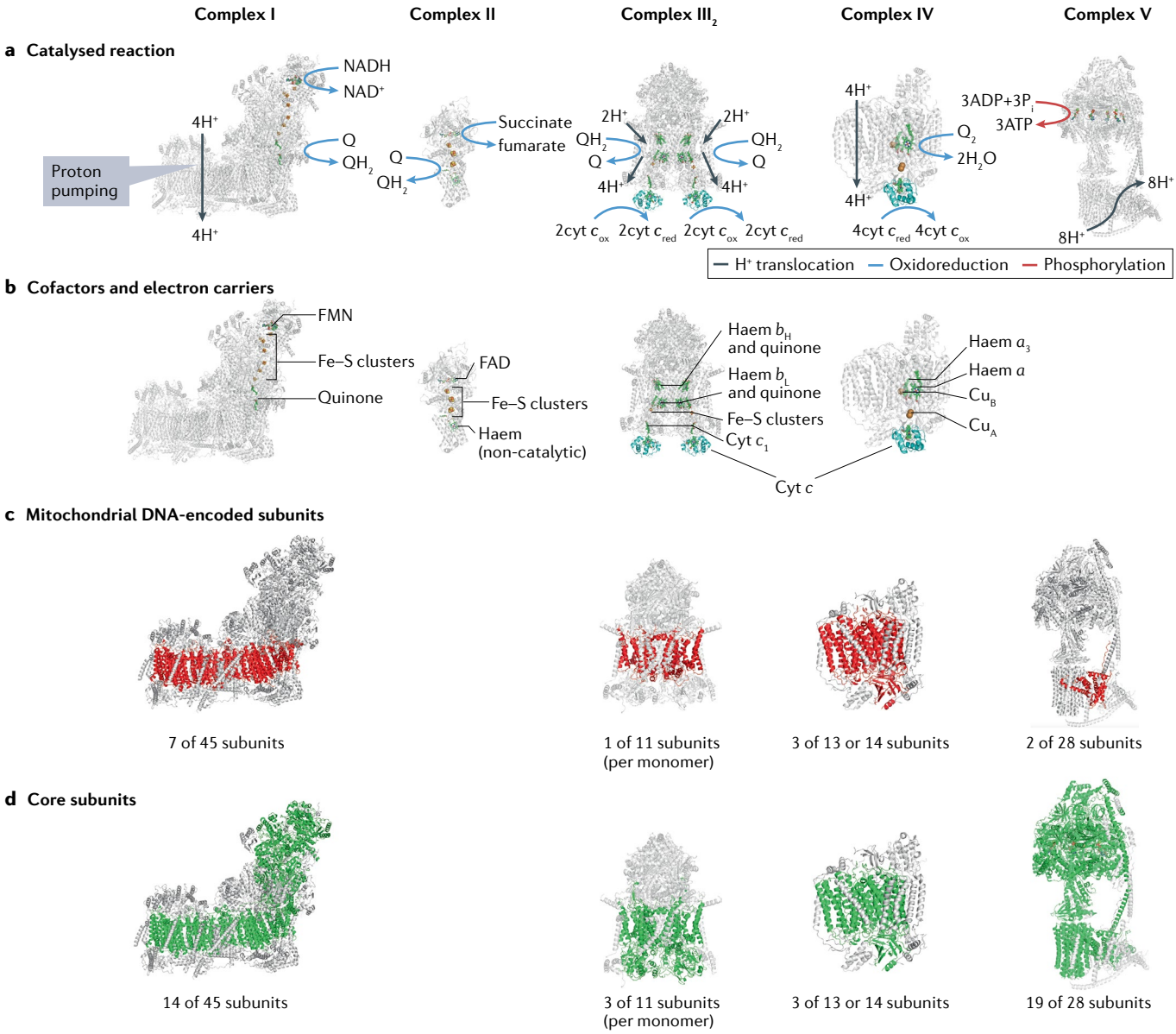

Fig. 2 | **Structural properties of the electron transport chain.** Atomic models of (left to right) complexes I (Protein Data Bank (PDB) ID 6ZKC), II (PDB ID 1ZOY), III_2 (PDB ID 6Q9E), IV (PDB ID 5IY5) and V (PDB ID 6TT7). **a** | Catalysed reactions, with reagents and products indicated (and cofactors shown as sticks/balls in the complexes, as described in part **b**). The soluble carrier cytochrome *c* (cyt *c*; PDB ID 3CX5 for complex III_2 and PDB ID 5IY5 for complex IV) is coloured in cyan. H^+ indicates protons, Q is the oxidized form of quinone, QH_2 is the reduced form of quinone. **b** | Cofactors bound to the complexes and electron carriers involved in electron transfer (flavin mononucleotide (FMN), iron–sulfur (Fe–S) clusters, FAD, haems, Cu centres and cytochromes), shown as sticks/balls and described next to each complex. Cyt *c* is shown as in part **a**. The non-catalytic haem bound to complex II is also indicated. **c** | Atomic models of complexes as in parts **a**,**b** with mitochondrial DNA-encoded subunits in red and nuclear DNA-encoded subunits in grey. The number of mitochondrial DNA-encoded subunits is indicated below, with reference to the total number of subunits in the complex. **d** | Atomic models of complexes as in parts **a**–**c** with core subunits in green and supernumerary subunits in grey. The number of core subunits is indicated below, with reference to the total number of subunits in the complex.

Table 1 | **Subunit composition of mitochondrial OXPHOS complexes**

Subunit name[a]	Core or supernumerary[b]	Gene origin	Cofactors	Assembly factors
Complex I				
NDUFV1 (51 kDa)	Core	Nuclear	FMN and N3 (4Fe–4S) cluster	ACAD9, ATP5SL, COA1, ECSIT, FOXRED1, NDUFAF1, NDUFAF2, NDUFAF3, NDUFAF4, NDUFAF5, NDUFAF6, NDUFAF7, NUBPL, TIMMDC1, TMEM70, TMEM126A, TMEM126B, TMEM186, TMEM261 (DMAC1)
NDUFV2 (24 kDa)	Core	Nuclear	N1a (2Fe–2S) cluster	
NDUFS1 (75 kDa)	Core	Nuclear	N1b (2Fe–2S), N4 (4Fe–4S) and N5 (4Fe–4S) clusters	
NDUFS2 (49 kDa)	Core	Nuclear	NA	
NDUFS3 (30 kDa)	Core	Nuclear	NA	
NDUFS7 (PSST)	Core	Nuclear	N2 (4Fe–4S) cluster	
NDUFS8 (TYKY)	Core	Nuclear	N6a (4Fe–4S) and N6b (4Fe–4S) clusters	
ND1	Core	Mitochondrial	NA	
ND2	Core	Mitochondrial	NA	
ND3	Core	Mitochondrial	NA	
ND4	Core	Mitochondrial	NA	
ND4L	Core	Mitochondrial	NA	
ND5	Core	Mitochondrial	NA	
ND6	Core	Mitochondrial	NA	
NDUFA1 (MWFE)	Supernumerary	Nuclear	NA	
NDUFA2 (B8)	Supernumerary	Nuclear	NA	
NDUFA3 (B9)	Supernumerary	Nuclear	NA	
NDUFA5 (B13)	Supernumerary	Nuclear	NA	
NDUFA6 (B14)	Supernumerary	Nuclear	NA	
NDUFA7 (B14.5a)	Supernumerary	Nuclear	NA	
NDUFA8 (PGIV)	Supernumerary	Nuclear	NA	
NDUFA9 (39 kDa)	Supernumerary	Nuclear	NA	
NDUFA10 (42 kDa)	Supernumerary	Nuclear	NA	
NDUFA11 (B14.7)	Supernumerary	Nuclear	NA	
NDUFA12 (B17.2)	Supernumerary	Nuclear	NA	
NDUFA13 (B16.6)	Supernumerary	Nuclear	NA	
NDUFAB1 (SDAP)	Supernumerary (present in two copies)	Nuclear	NA	
NDUFB1 (MNLL)	Supernumerary	Nuclear	NA	
NDUFB2 (AGGG)	Supernumerary	Nuclear	NA	
NDUFB3 (B12)	Supernumerary	Nuclear	NA	
NDUFB4 (B15)	Supernumerary	Nuclear	NA	
NDUFB5 (SGDH)	Supernumerary	Nuclear	NA	
NDUFB6 (B17)	Supernumerary	Nuclear	NA	
NDUFB7 (B18)	Supernumerary	Nuclear	NA	
NDUFB8 (ASHI)	Supernumerary	Nuclear	NA	
NDUFB9 (B22)	Supernumerary	Nuclear	NA	
NDUFB10 (PDSW)	Supernumerary	Nuclear	NA	
NDUFB11 (ESSS)	Supernumerary	Nuclear	NA	
NDUFC1 (KFYI)	Supernumerary	Nuclear	NA	
NDUFC2 (B14.5b)	Supernumerary	Nuclear	NA	
NDUFS4 (18 kDa/ AQDQ)	Supernumerary	Nuclear	NA	
NDUFS5 (15 kDa/PFFD)	Supernumerary	Nuclear	NA	
NDUFS6 (13 kDa)	Supernumerary	Nuclear	NA	
NDUFV3 (10 kDa)	Supernumerary	Nuclear	NA	

Table 1 (cont.) | **Subunit composition of mitochondrial OXPHOS complexes**

Subunit name[a]	Core or supernumerary[b]	Gene origin	Cofactors	Assembly factors
Complex II				
SDHA	Core	Nuclear	FAD	SDHAF1, SDHAF2, SDHAF3, SDHAF4
SDHB	Core	Nuclear	2Fe–2S, 4Fe–4S and 3Fe–4S clusters	
SDHC	Core	Nuclear	NA	
SDHD	Core	Nuclear	NA	
Complex III$_2$				
UQCRC1 (core 1)	Supernumerary	Nuclear	NA	BCS1L, UQCC1, UQCC2, UQCC3, HIGD1A, LYRM7, TTC19, BRAWNIN
UQCRC2 (core 2)	Supernumerary	Nuclear	NA	
MT-CYB (cytochrome b_1)	Core	Mitochondrial	Haem b_L/b_H	
CYC1 (cytochrome *c*)	Core	Nuclear	Haem c_1	
UQCRFS1 (ISP)	Core	Nuclear (the precursor is shared with subunit 9: the carboxy terminus becomes ISP)	2Fe–2S cluster	
UQCRB	Supernumerary	Nuclear	NA	
UQCRQ	Supernumerary	Nuclear	NA	
UQCRH	Supernumerary	Nuclear	NA	
UQCR10	Supernumerary	Nuclear	NA	
UQCR11	Supernumerary	Nuclear	NA	
Subunit 9	Supernumerary	Nuclear (the precursor is shared with ISP: the N terminus becomes subunit 9)	NA	
Complex IV				
MT-CO1	Core	Mitochondrial	Cu_B, Mg^{2+}, Haem a/a_3	CEP89, CMC1, CMC2, COA1, COA2, COA3, COA5, COA6, COA7, COA8, COX10, COX11, COX14, COX15, COX16, COX17, COX18, COX19, COX20, COX23, COX24, FASTKD2, HIGD1A, HIGD2A, IMP1, IMP2, LRPPRC, MITRAC7, MDJ1, MR-1S, MSS2, OMA1, OXA1, PET54, PET100, PET111, PET117, PET122, PET494, PNT1, SCO1, SCO2, SOM1, SSC1, SURF1, TACO1, TMEM177
MT-CO2	Core	Mitochondrial	Cu_A	
MT-CO3	Core	Mitochondrial	NA	
COX4	Supernumerary	Nuclear	NA	
COX5A	Supernumerary	Nuclear	NA	
COX5B	Supernumerary	Nuclear	Zn^{2+}	
COX6A	Supernumerary	Nuclear	NA	
COX6B	Supernumerary	Nuclear	NA	
COX6C	Supernumerary	Nuclear	NA	
COX7B	Supernumerary	Nuclear	NA	
COX7C	Supernumerary	Nuclear	NA	
COX8B	Supernumerary	Nuclear	NA	
COX7A	Supernumerary	Nuclear	NA	
NDUFA4	Supernumerary	Nuclear	NA	
Complex V				
α (ATP5A1)	Core (present in three copies)	Nuclear	NA	ATPAF1, ATPAF2, C7orf55, TMEM70, TMEM242 (ATP10P and ATP23P identified in yeast[169])
β (ATP5B)	Core (present in three copies)	Nuclear	NA	
γ (ATP5C1)	Core	Nuclear	NA	
δ (ATP5D)	Supernumerary	Nuclear	NA	

Table 1 (cont.) | **Subunit composition of mitochondrial OXPHOS complexes**

Subunit name[a]	Core or supernumerary[b]	Gene origin	Cofactors	Assembly factors
Complex V (cont.)				
ε (ATP5E)	Core	Nuclear	NA	
OSCP (ATP5O, δ in bacteria)	Core	Nuclear	NA	
b (ATP5F1)	Core	Nuclear	NA	
F_6 (ATP5J)	Supernumerary	Nuclear	NA	
d (ATP5H)	Supernumerary	Nuclear	NA	
a (MT-ATP6, ATP6)	Core	Mitochondrial	NA	
ATP8 (MT-ATP8, A6L)	Supernumerary	Mitochondrial	NA	
DAPIT (USMG5)	Supernumerary	Nuclear	NA	
6.8PL (C14orf2)	Supernumerary	Nuclear	NA	
f (ATP5J2)	Supernumerary	Nuclear	NA	
c (ATP5G1, ATP5G2, ATP5G3)	Core (present in eight copies in mammals)	Nuclear (in plants and animal). In yeast it is encoded in the mitochondrial DNA[170]	NA	
e (ATP5I)	Supernumerary	Nuclear	NA	
g (ATP5L)	Supernumerary	Nuclear	NA	

FMN, flavin mononucleotide; ISP, Rieske iron–sulfur protein; NA, not applicable; OXPHOS, oxidative phosphorylation. [a]Commonly used aliases are indicated in parentheses. [b]If multiple copies are present in the final complex, this is indicated in parentheses.

disorders have been linked to mutations in assembly factors[20,21], thereby highlighting their crucial role in cell metabolism. As a further layer of complexity, the single ETC components have been found to gather into so-called supercomplexes of different stoichiometry[22–32] (FIG. 1a, inset on the right), which have recently been shown to be crucial for the correct assembly of the individual complexes[33,34], thereby implying a novel mechanism of self-regulation of the assembly of OXPHOS complexes. As the function of the ETC relies on the supply of reducing equivalents — generated through cell metabolism — it is deeply connected to the metabolic state of the cell (and even the entire organism) (BOX 1).

It is of paramount importance to understand how the components of the OXPHOS system work and how they are regulated, as their malfunction inevitably leads to severe diseases such as neurodegenerative disorders and cancer[35], in addition to being linked to ageing[36]. The assembly pathways of the OXPHOS system components, together with the diseases associated with them, were recently extensively reviewed elsewhere[37,38] (see also BOX 2). In the past few years, a great deal of information from different fields has been published about the detailed mechanism of action of the respiratory chain complexes[30,39–44], as well as their assembly and regulation, mainly via the association in the supercomplexes[33,34]. This Review aims to outline the newest findings in this area, as well as to highlight the remaining open questions, which are currently directing the research in the field. We describe the assembly of the single complexes, alone and in relation to the formation of supercomplexes. We also briefly describe their catalytic mechanisms, highlighting new structural data. We discuss the function of supercomplexes in light of the regulation of the ETC, depending on the metabolic needs of the cells, as imposed by the environment or by the tissue specificity.

ETC organization and activity

As mentioned in the introduction, the components of the ETC are complex macromolecular structures composed of protein subunits as well as different types of cofactors (FIG. 2). Despite the extensive effort made in the field, crucial questions remain to fully elucidate their mechanism of assembly and their mechanism of action. In this section we therefore discuss these processes. We specifically focus on describing the structural features of the individual OXPHOS complexes and reviewing the state-of-the-art knowledge of their mechanisms of activity emerging from this structural picture, and we include highlights of the most relevant future perspectives for understanding the function of this complex mitochondrial respiration machinery.

Assembly, structure and mechanism of complex I. Complex I is the largest component of the respiratory chain, with a total mass of approximately 1 MDa in mammals, being composed of 14 core subunits and 31 supernumerary subunits[25,45,46]. The seven membrane-embedded core subunits (ND1–ND6 and ND4L) are encoded in the mitochondrial genome[47,48]. The core subunits constitute the innermost part of complex I and harbour all the catalytic sites. The hydrophilic arm (also known as the peripheral or matrix arm), where NADH oxidation occurs, contains core subunits NDUFS1, NDUFV1, NDUFS2, NDUFV2, NDUFS3, NDUFS7 and NDUFS8, as well as the primary electron acceptor flavin mononucleotide and eight Fe–S clusters[49].

E-channel
Group of charged residues (mostly glutamates (E)) located within subunits ND1, ND3, ND6 and ND4L of the complex I membrane arm involved in the coupling mechanism of quinone reduction to proton translocation.

Brown adipose tissue
Subtype of fat tissue characterized by a dark colour, as opposed to the normal white appearance, devoted to thermogenesis (via the uncoupling of proton gradient dissipation from ATP synthesis) instead of energy storage. Brown adipose tissue thus contains a lot more (brown) mitochondria than (white) lipid droplets.

Seven of the Fe–S clusters connect the NADH-binding site and the quinone-binding site (Q site), while cluster N1a is off this main electron transfer pathway. The membrane arm features subunits ND1, ND3, ND4L and ND6, which form a putative proton translocation pathway (E-channel) close to the Q site and three homologous antiporter-like subunits ND2, ND4 and ND5, whose structural organization resembles that of cation/H^+ antiporters and which are thought to hold a proton channel each (FIG. 2). The core subunits are encaged, both in the matrix and in the membrane, by a network of supernumerary subunits, which are important for assembly and stability of the complex[19] (listed in TABLE 1).

In addition to the 45 structural subunits of complex I, almost 20 assembly factors participate in its biogenesis[37,50,51]. Complex I assembly starts from the independent formation of six modules (FIG. 3a): N (NDUFV1, NDUFV2, NDUFS1 and NDUFA2; components of the peripheral NADH-oxidizing part of the matrix arm), Q (NDUFA5, NDUFS2, NDUFS3, NDUFS7 and NDUFS8; components of the matrix arm towards the interface with the membrane arm and forming part of the Q site), P_P-a (ND1, NDUFA3, NDUFA8 and NDUFA13; components of the membrane-embedded portion of the Q site), P_P-b (ND2, NDUFC1, NDUFC2, ND3, ND4L and ND6; components of the E-channel and of the first antiporter-like subunit), P_D-a (NDUFB5, NDUFB10, NDUFB11, NDUFB6 and ND4; components around the second antiporter-like subunit) and P_D-b (NDUFAB1 (also known as mitochondrial acyl carrier protein), NDUFB7, NDUFB3, NDUFB8, ND5, NDUFB9 and NDUFB2; components around the third antiporter-like subunit). Subsequently, the separate modules come together, with P_D-a and P_P-a accompanied by Q associating with P_P-b, followed by addition of P_D-b. The N module is the last to be added. Subunits NDUFA1 of the P_P-a module, NDUFA10 and NDUFS5 of the P_P-b module, NDUFB1 and NDUFB4 of the P_D-a module, NDUFA9, NDUFA7, NDUFA11, NDUFAB and NDUFA6 of the Q module and NDUFS4, NDUFV3, NDUFA12 and NDUFS6 of the N module are added at different stages of the module association and are not part of the initial, separate modules[51].

Various assembly factors are known to participate in the assembly of complex I. The assembly of the Q module is assisted by the assembly factors NUBPL (also assisting the N module) and NDUFAF3–NDUFAF7. Assembly of the membrane-embedded P modules is aided by the assembly factor TIMMDC1 for the P_P-a module, by FOXRED1, ATP5SL, TMEM126A[52] and TMEM70 for the P_D-a module (although the role of TMEM70 is controversial, as it has also been shown to play a role in the assembly of complex V (REF.[53,54])), by ACAD9, ECSIT, NDUFAF1, COA1 (also involved in complex IV biogenesis[55]), TMEM126B and TMEM186 for the P_P-b module and by DMAC1 for the P_D-b module. Except for

Box 1 | Regulation of the electron transport chain in tune with metabolism

The primary determinant of the function of the electron transport chain (ETC) is the ADP:ATP ratio, reflecting the metabolic needs of the cell in terms of ATP consumption (energy requirements)[171,172]. The respiration rate is therefore high at high ADP:ATP ratios — that is, when cells are consuming ATP (named 'state 3 of respiration') — whereas it drops in state 4, upon decrease of the ADP:ATP ratio[173]. The phosphorylation of ADP in state 3 is tightly coupled to the reduction of oxygen, allowing the establishment of the transmembrane electrochemical gradient[174]. The important exception to this is thermogenesis, a process occurring in brown adipose tissue, by which the ETC-produced electrochemical potential is dissipated by uncoupling proteins[175] to generate heat[176].

Another way to regulate the ETC is by tuning the availability of NADH and succinate, the reducing equivalents that act as inputs to complex I and complex II. Three recent publications have finally identified SLC25A51 as the mitochondrial NADH importer[177–179] (see also REF.[180] for a review). After pathways for mitochondrial synthesis of NAD^+ (REF.[181]) had been ruled out, it was clarified that NAD^+ is imported via SLC25A51, which was found to be necessary and sufficient to supply mitochondria with NAD^+ and able to rescue the ablation of the yeast, non-homologous, transporter in knockout cells. Further studies on the regulation of SLC25A51 activity and its mechanism of transport as well as the investigation of potential additional players in NAD^+ import are now needed to enrich our knowledge of this fundamental biochemical process in the context of cellular metabolism. Additionally, this will pave the way for new studies on the regulation of complex I activity through the availability of its electron donor. In addition to its role in cancer and inflammation, as discussed in BOX 2, succinate has also been recently found to regulate thermogenesis in brown adipose tissue: the study authors propose that this occurs via increased succinate oxidation by complex II, with a concomitant increase in the production of reactive oxygen species, which would in turn stimulate thermogenesis[182].

Even more upstream of the electron donors, the availability of nutrients has a profound impact on the function of the ETC. Mitochondrial respiration produces ATP downstream of the Krebs cycle, which utilizes acetyl-CoA as the initial substrate[3]. In turn, acetyl-CoA can be derived from both sugar (via glycolysis) and fatty acid (via fatty acid β-oxidation) metabolism, with an important difference: while glycolysis yields two molecules of acetyl-CoA per six carbon atoms of the initial substrate, fatty acid β-oxidation yields three[183], meaning that the efficiency of ATP production by the oxidative phosphorylation (OXPHOS) system is higher if the energy source is fat as opposed to sugar. On the other hand, glycolysis can be a fundamental energy-producing pathway per se, as in anaerobic conditions (that is, when the OXPHOS system is inhibited) it can still produce ATP (although only two molecules per glucose molecule via glycolysis and lactic fermentation[184] versus the 27.5–28.9 produced by respiration[185]) and has long been found to be a pillar for tumour growth, via the Warburg effect[186], according to which cancer cells display high rates of glucose utilization, coupled to lactate excretion, even in aerobic conditions[187]. Regarding the interplay between different metabolic routes for ATP production, a noteworthy recent study[188] attempted to identify the key players in the regulation of ATP homeostasis via CRISPR-based genetic screening in different metabolic conditions: importantly, the study authors evidenced a mutual regulation between OXPHOS and glycolysis. While the knockdown of the early glycolytic enzyme hexokinase 2 (HK2) expectedly correlated with a decrease in the levels of downstream metabolites under glycolytic conditions, in respiratory conditions it boosted ATP production via the Krebs cycle and the OXPHOS system.

In addition to nutrients, at the other end of the chain, playing a crucial role in the ETC regulation, is oxygen. On the one hand, oxygen availability determines the ETC function as the final electron acceptor and in turn mitochondria function as oxygen sensors in cells, modulating the ADP:ATP ratio in response to oxygen concentration[189]. The scarcity of oxygen determines the pathological condition of hypoxia, whose effects on cellular homeostasis, including the ETC function, were recently reviewed[190]. Importantly, oxygen is also the substrate for the formation of reactive oxygen species: as discussed in the main text, the ETC components are a major source of the electrons that generate oxygen radicals.

Box 2 | **Deregulation of the electron transport chain in disease**

Mitochondrial disorders are a group of genetic diseases that affect the mitochondrial function. While each of them is rare, taken together they affect 5–15 people per 100,000 at birth and 3–10 per 100,000 adults[191]. Given the central role of the electron transport chain (ETC) in mitochondrial energy production, a plethora of mutations in its components have been connected with mitochondrial disorders, especially affecting tissues that rely on high levels of ATP, such as the brain and the skeletal muscle (thus causing encephalocardiomyopathies)[192] and the subject has been extensively reviewed[193–195]. Prominent examples[196] of syndromes linked to mitochondrial malfunction include Leigh syndrome, which is related to mutations of more than 75 genes[197], MELAS (mitochondrial encephalomyopathy with lactic acid and stroke-like episodes) syndrome, which is commonly linked to mutations in the gene encoding $tRNA^{Leu(UUR)}$ (REF. [198]) and Leber hereditary optic neuropathy[199], which is caused by mutations in complex I subunits[200]. Aside from the aforementioned syndromes, in the panorama of disease-related mutations, complex II stands out, as its substrate, succinate, has been defined as an oncometabolite, thereby making complex II a tumour suppressor[201–203]. Briefly, accumulation of succinate due to loss-of-function mutations in complex II induces histone and cytosine hypermethylation, which in turn disrupts the epigenetic control of gene expression, thereby promoting crucial cancer-related phenotypes such as epithelial–mesenchymal transition, cell migration and invasiveness. In addition, succinate inhibits the enzyme prolyl hydroxylase (PHD), which is involved in the degradation of the transcription factor hypoxia-inducible factor 1α (HIF1α). The resulting stabilization of HIF1α sustains tumour progression via the stimulation of angiogenesis, the metabolic switch from respiration to glycolysis and the secretion of IL-1β. It is therefore not surprising that mutations in complex II components have been associated with different cancer types, such as paragangliomas and phaeochromocytomas, gastrointestinal stromal tumours and renal cell carcinomas. Succinate is also involved in the inflammatory response via the HIF1α-driven stimulation of macrophages to produce proinflammatory cytokines[204,205]. Importantly, an increase in succinate concentration was found to lead to a boost in complex II activity, with accompanying increase in the production of reactive oxygen species and consequential downstream activation of HIF1α[206]. In addition to complex II, complex I-mediated production of reactive oxygen species was found to contribute to the proinflammatory phenotype[205]. In this respect, it is also worth mentioning that complex III_2 is another key player in the regulation of inflammation, via its role in the maintenance of the specific regulatory function of regulatory T cells[207]. In addition to the enzymatic complexes and the electron donors, the deregulation of the two mobile electron carriers, the membrane-embedded ubiquinone and the soluble cytochrome *c*, has severe consequences for metabolism. Ubiquinone deficiencies have long been linked to severe neuromuscular symptoms, similarly to the loss-of-function mutations that occur in the enzymatic complexes themselves[208–210]. In addition, complex II-driven production of reactive oxygen species was recently linked to loss of ubiquinone in models of insulin resistance[208]. Interestingly, a recent publication[211] also showed that complex III_2 is necessary to sustain tumour growth, via oxidation of the quinone pool. The study authors confirmed that oxidized quinone is required to maintain cancer cells, thereby paving the way for novel potential anticancer strategies aimed at keeping the quinone pool reduced. Cytochrome *c*, instead, has a dual role in cell homeostasis: in mitochondria, it shuttles electrons from complex III_2 to complex IV, whereas when released to the cytosol, it triggers apoptosis[212] by activating the caspase chain[213]. These two opposite effects were elegantly investigated in a study where cytochrome *c* deletion in mouse models resulted in fetal lethality, due to the inability of the embryos to undergo the metabolic switch between glycolysis and mitochondrial respiration, as electrons stall at complex III_2. However, cells derived from the embryos could be rescued by supplementing them with uridine and pyruvate to make up for the loss of oxidative phosphorylation-derived ATP. This supplementation not only allowed them to survive, but actually increased their resistance to apoptosis[214].

the specific references indicated above, the roles of the assembly factors mentioned are outlined in REFS[37,38,51].

Functionally, complex I couples the reduction of quinone by NADH to the pumping of four protons across the IMM (from the mitochondrial matrix into the intermembrane space (IMS)). The oxidoreduction reaction occurs in the matrix arm, while the protons are pumped through the membrane arm (FIG. 2a). For complex I to function, these two actions have to be precisely concerted, and the mechanism by which this happens has been hotly debated. Complex I catalysis starts from the oxidation of NADH to NAD^+ at the top of the matrix arm[56]: while one proton is released in the matrix, the two electrons tunnel through a chain of Fe–S clusters along the matrix arm to the junction with the membrane arm, where the N2 cluster donates them to ubiquinone[57]. The oxidoreduction mechanism was first revealed by biochemical[58] and structural[59] studies of the bacterial enzyme and later confirmed to be conserved in mammals when their cryo-electron microscopy (cryo-EM) structures became available. Recent yeast[60], murine[61] and bacterial[41] structures revealed the binding modes of quinones and quinone-like inhibitors within the Q site, a long and narrow cavity linking the quinone entry site, exposed to the lipid bilayer, and the quinone reduction site at the deep end of the cavity near Fe–S cluster N2. High-resolution ovine structures[40] clarified the quinone binding modes under turnover conditions (that is, in presence of excess of substrates, so that the enzyme performs catalytic cycles until flash-frozen), as well as the coupling mechanism, linking the quinone reduction to the proton translocation. The ovine structures revealed the absence of any conformational changes in the antiporters (subunits ND2, ND4 and ND5) under full turnover conditions[40], in contrast to the observed large-scale movements around the Q site, linking quinone chemistry to proton pumping. Likewise, no change in the antiporter area has been observed in the currently available structures from other species[60]. This suggests that proton pumping in the antiporters is mainly electrostatically driven, as proposed earlier in electrostatic wave-type mechanisms[62,63] (for a more detailed overview of the mechanism of complex 1 activity emerging from these structures, see BOX 3). Further details of proton pumping remain elusive. It was initially proposed that for each functional cycle, one proton would travel through the E-channel and the other three would pass through each of the antiporter subunits[49]. However, this notion has been questioned, as no water molecules or any other connections to the IMS were identified in the ND2 and ND4 subunits[40]. Therefore, the proton output into the IMS appears to occur only through ND5. Nevertheless, all or most antiporters could participate in the uptake of protons from the matrix, with protons then redistributed towards ND5 via the hydrophilic central axis, which is composed of

Oncometabolite
Substrate of metabolic reactions whose aberrant accumulation triggers cancer-related pathways.

Epithelial–mesenchymal transition
Biological process typical of embryonic development, but also observed in cancer, by which epithelial cells acquire mesenchymal properties (for example, losing apicobasal polarity and increasing their motility).

Paragangliomas and phaeochromocytomas
Paragangliomas are a rare type of neuroendocrine cancer growing around ganglia (groups of neuronal bodies and glial cells) in the head, neck, torso and abdomen. Specifically, when affecting the adrenal glands, they are called 'phaeochromocytomas'.

Insulin resistance
Pathological condition in which cells do not respond to insulin, thereby not internalizing and utilizing glucose. This phenomenon is correlated with the development of type 2 diabetes.

Caspase
Refers to a family of proteases activated by various stimuli and responsible for the apoptotic response in cells.

Electrostatic wave
Mechanism of signal transduction along the membrane arm of complex I by which the change in the charge status of key polar residues drives proton translocation.

Midpoint potential
Electric potential at which the oxidized and reduced components of a redox reaction are at equilibrium (that is, the midpoint of a redox titration).

Rieske iron–sulfur protein
(ISP). Membrane-anchored catalytic subunit of complex III_2 shuttling electrons from quinol bound at haem b_L to cytochrome c_1 via its iron–sulfur cluster.

Low-potential redox chain
A pathway for electron transfer within complex III_2 which goes from haem b_L to haem b_H. It shows low redox potential.

High-potential redox chain
A pathway for electron transfer within complex III_2 that goes from the ISP to cytochrome c_1. It shows high redox potential.

Electron paramagnetic resonance
Spectroscopic technique detecting unpaired electrons by the application of a magnetic field. In bioenergetics, it is used to study radicals, such as the quinone intermediates between fully oxidized and fully reduced states, as well as the electron transfer through transition metals in iron–sulfur clusters, haems and copper centres.

conserved hydrophilic residues located in the middle of the membrane arm and spanning its full length[40]. Structures resolved in the presence of proton-motive force and/or using time-resolved techniques to trap short-lived transition states of the complex will help to elucidate the proton transfer mechanism so as to rule out any so far unobserved conformational changes and verify the details of electrostatic interactions between key charged residues.

Assembly, structure and mechanism of complex II. Complex II is a crucial player in cellular metabolism, given its position at the intersection between two key pathways, the Krebs cycle and the OXPHOS system[8]. Complex II couples the oxidation of succinate to fumarate (in the Krebs cycle) with the reduction of ubiquinone to ubiquinol, thereby contributing to the reduction of the quinone pool, the substrate of complex III_2 of the ETC (FIG. 1).

Complex II is composed of four subunits, all of which are encoded in the nuclear genome[8]. The soluble subunits SDHA and SDHB contain the covalently bound FAD, the primary electron acceptor in the complex, and three Fe–S clusters (2Fe–2S, 4Fe–4S and 3Fe–4S), which are responsible for oxidation of succinate and electron transfer to quinone. These two matrix-located subunits are linked to the IMM via membrane-embedded subunits SDHC and SDHD. The quinone binds to and is reduced[64] at the interface formed by SDHB, SDHC and SDHD, whereas between SDHC and SDHD a haem group is bound; this haem group has no catalytic function but is important for assembly and stability of the membrane part of the complex[65] (FIG. 2a,b).

The assembly of the matrix subunits is assisted by four SDHAF assembly factors: SDHAF1–SDHAF4. The assembly process for complex II was recently reviewed[37,38,66]. Briefly, cofactors are loaded in parallel onto SDHA and SDHB, whereas SDHC and SDHD dimerize in the membrane. The soluble subunits then associate and finally bind to the SDHC–SDHD subcomplex to form a full complex II (FIG. 3a). It is important to note that two binding sites for quinone have been described on the basis of structural data, one on the matrix side (sometimes referred to as the proximal side) and one on the IMS side (also known as the distal side) of the IMM[65]. On the basis of further structural[67] and biochemical [68,69] data, though, it appears that only the matrix site is catalytically relevant, as the IMS site is too far away from the Fe–S cluster for electron transfer and the haem at the interface between SDHC and SDHD does not transfer electrons[70,71].

The mechanism of action of complex II involves oxidation of succinate ($C_4H_6O_4$) to fumarate ($C_4H_4O_4$) in the SDHA subunit: the covalent bond of FAD is crucial to raise the midpoint potential of the reaction and favour succinate oxidation[72]. While the two protons resulting from succinate oxidation are released into the matrix, the electrons are passed on to the three Fe–S clusters in SDHB and then on to the ubiquinone bound to SDHC and SDHD[69]. Because the reduction of quinone involves two protons derived from the matrix side, no net proton exchange across the IMM is associated with the oxidoreduction activity of complex II (FIG. 2). The exact path through which protons are transferred through complex II to result in ubiquinone reduction is still unknown[64].

Assembly, structure and mechanism of complex III_2. Complex III_2 couples ubiquinol oxidation to reduction of the soluble electron carrier cytochrome *c*, while taking up two protons from the matrix and releasing four into the IMS (FIGS 1a,2a); it has an obligate homodimeric structure, related to its function, with three catalytic subunits per monomer (or protomer) that are highly conserved from bacteria to eukaryotes: cytochrome *b* (also known as MT-CYB), the only mitochondrial DNA-encoded subunit, cytochrome c_1 (also known as CYC1) and the Rieske iron–sulfur protein (ISP; also known as UQCRFS1)[18]. Cytochrome *b* contains two haem groups, named haem b_L and haem b_H, constituents of the low-potential redox chain, whereas cytochrome c_1 harbours haem c_1, a constituent of the high-potential redox chain along with the Fe–S cluster in the Rieske protein (FIG. 2b).

The mechanism of action of complex III_2 is referred to as the Q cycle, and it involves the concerted action of both protomers[5,6], as the ISP subunit of every protomer transfers electrons from quinone bound at cytochrome b_L (in the so-called *b*, or proximal, conformation) to cytochrome c_1 (in the so-called *c*, or distal, conformation) of the opposite protomer[73]. Thus, each protomer of the complex III_2 enzyme is in principle active, but the Q cycle can be performed only in the dimeric form. The Q cycle begins with the binding of one quinol at the haem b_L site. From there, the first electron and the first proton are donated to the Fe–S cluster and a conserved histidine of ISP, respectively (rate-limiting step of the reaction). This generates a highly reactive quinone radical, which eventually is fully oxidized by haem b_L. From haem b_L, the electron is passed to haem b_H and then to an oxidized quinone at the haem b_H site. The partially reduced quinone at the haem b_H site is then fully reduced to quinol when the cycle described is repeated[18]. A key feature of the mechanism is the electron bifurcation at haem b_L, which allows the reduction of cytochrome *c* and quinone at opposite sides of the complex, coupled to the complete oxidation of one quinol molecule[74]. The first electron is donated to the ISP, due to the higher potential of the Fe–S cluster and haem c_1 compared with haems *b*[75], while the second electron can follow the low-potential chain once the ISP has moved from the *b* position to the *c* position, where the electron is transferred to cytochrome c_1 (REF.[18]). Cytochrome c_1 then passes the electron to the soluble electron carrier cytochrome *c*. For completion of the cycle, two quinols are oxidized at the haem b_L site at the IMS side, thereby reducing two cytochrome *c* molecules through the ISP and cytochrome c_1 and regenerating one quinol at the haem b_H site at the matrix side[18]. The exact kinetics of the Q cycle has been extensively studied by electron paramagnetic resonance measurements: the extreme instability of the intermediates and the big movements associated with ISP-driven electron transfer to cytochrome *c* make it difficult to obtain structures of the catalytic intermediates[76–82].

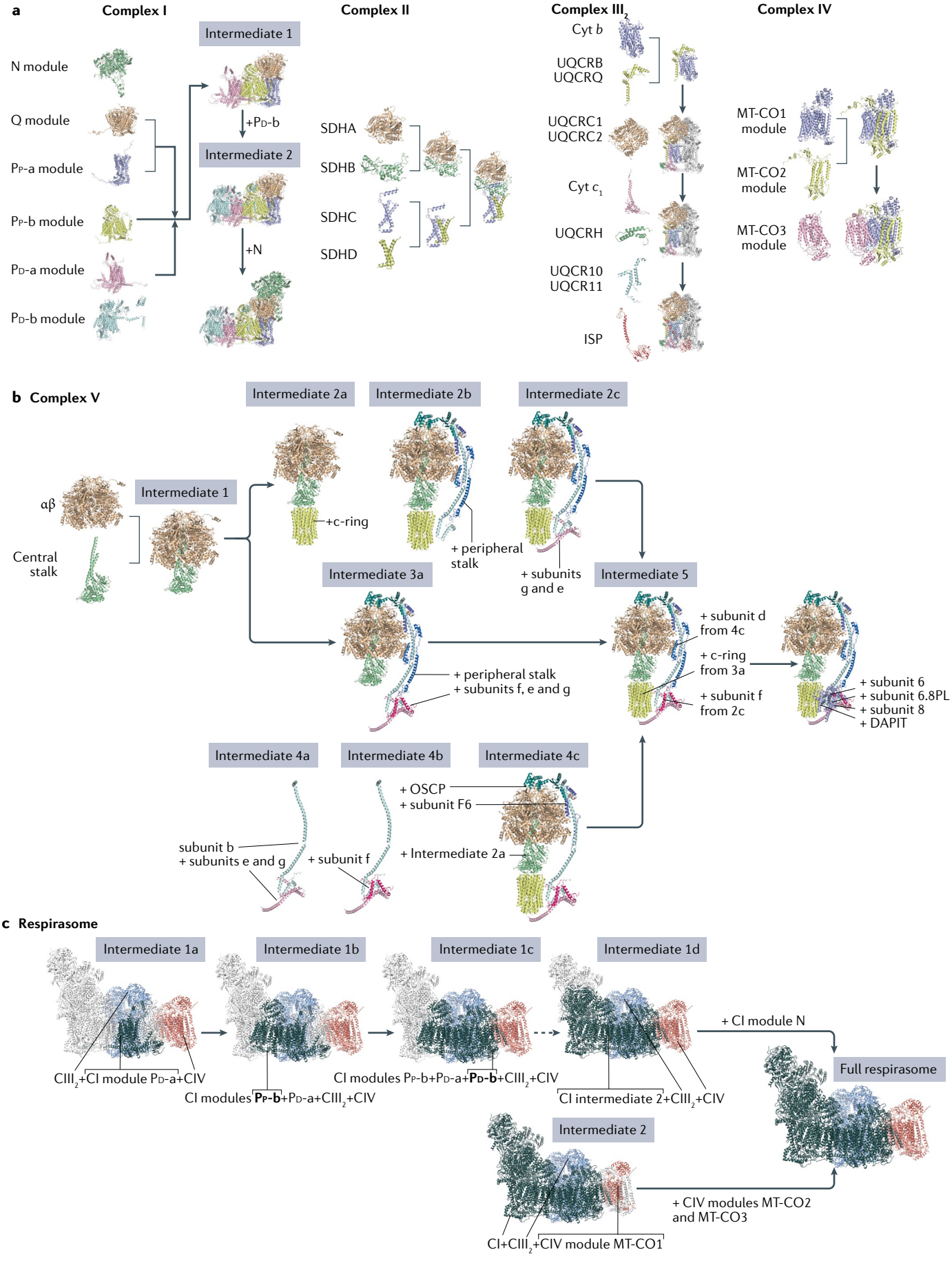
a
Complex I
Intermediate 1
N module
Q module
PP-a module
PP-b module
PD-a module
PD-b module
+PD-b
Intermediate 2
+N
Complex II
SDHA
SDHB
SDHC
SDHD
Complex III2
Cyt b
UQCRB
UQCRQ
UQCRC1
UQCRC2
Cyt c1
UQCRH
UQCR10
UQCR11
ISP
Complex IV
MT-CO1 module
MT-CO2 module
MT-CO3 module
b Complex V
Intermediate 2a
Intermediate 2b
Intermediate 2c
αβ
Central stalk
Intermediate 1
+c-ring
+ peripheral stalk
+ subunits g and e
Intermediate 3a
Intermediate 5
+ peripheral stalk
+ subunits f, e and g
+ subunit d from 4c
+ c-ring from 3a
+ subunit f from 2c
+ subunit 6
+ subunit 6.8PL
+ subunit 8
+ DAPIT
Intermediate 4a
Intermediate 4b
Intermediate 4c
subunit b
+ subunits e and g
+ subunit f
+ OSCP
+ subunit F6
+ Intermediate 2a
c Respirasome
Intermediate 1a
Intermediate 1b
Intermediate 1c
Intermediate 1d
CIII2+CI module PD-a+CIV
CI modules PP-b+PD-a+CIII2+CIV
CI modules PP-b+PD-a+CIII2+CIV
CI intermediate 2+CIII2+CIV
+ CI module N
Full respirasome
Intermediate 2
+ CIV modules MT-CO2 and MT-CO3
CI+CIII2+CIV module MT-CO1

◀ Fig. 3 | **Assembly process of respiratory complexes and supercomplexes.** Atomic models of the electron transport chain components as in FIGS 1,2: complexes I (Protein Data Bank (PDB) ID 6ZKC), II (PDB 1ZOY), III_2 (dimeric complex III; PDB ID 6Q9E), IV (PDB ID 5IY5) and V (PDB ID 6TT7). For the respirasome, the individual complexes (PDB IDs listed above) were docked into the cryo-electron microscopy map (EMD-8130) of the ovine respirasome due to higher completeness of the atomic model compared with the respirasome model (PDB ID 5J4Z). **a** | Assembly of respiratory complexes I, II, III_2 and IV (PDB IDs listed above). Assembly modules, or individual subunits, are indicated. Membrane-embedded modules are coloured light blue, light pink, yellow, red, lilac and pale cyan, and soluble modules are coloured pale green and wheat. For complex III_2, the second monomer is depicted in grey. **b** | Assembly of ATP synthase (complex V; PDB ID listed above). Given the complexity of the assembly, additional colours are used. **c** | Assembly of the respirasome according to the current models described in the main text (PDB IDs listed above). Top: assembly of intermediates of complex I (CI) with full complexes III_2 ($CIII_2$) and IV (CIV). These are labelled as sequential intermediates 1. For intermediates 1b and 1c, the added module of complex I is highlighted in bold and indicated in the structure. Bottom: assembly of full complexes I and III_2 and the MT-CO1 module of complex IV (termed 'intermediate 2'). For clarity, the full respirasome model is shown in every step, with the missing parts in each step coloured in light grey. The dashed arrow indicates that there are missing, putative sequential intermediates involving the P_P-a and Q modules that have not been identified so far. ISP, Rieske iron–sulfur protein.

In addition to the catalytic subunits, complex III_2 contains supernumerary subunits, whose composition differs across species, with the mammalian enzyme containing eight such subunits: the so-called core 1 and core 2 proteins (a traditional name, they are not part of the catalytic core; they are also known as UQCRC1 and UQCRC2) in the matrix and six additional supernumerary subunits, five of which encapsulate the catalytic core (UQCRH, UQCRB, UQCRQ, UQCR10 and UQCR11)[18] and one of which (subunit 9) corresponds to the cleaved signal peptide from the ISP precursor, and has been shown to be caged in the cavity between the core proteins[83].

The assembly process was recently reviewed[84] (see also FIG. 3a for an overview). In brief, the complex assembly starts from the insertion of monomeric cytochrome *b* in the membrane and its association with haems b_H and b_L, assisted by the assembly factors UQCC1, UQCC2 and UQCC3 (REF.[85]). UQCRQ and UQCRB then join and stabilize the mature cytochrome *b*, forming a stable intermediate (known as intermediate II)[86]. At this stage, UQCRC1 and UQCRC2 are incorporated on the matrix side, while cytochrome c_1 and UQCRH join at the IMS side, thereby forming a dimeric intermediate III. It was recently shown that in yeast a tetramer of core proteins (UQCRC1–UQCRC2 dimer) attaches to two preformed intermediates II, with cytochrome c_1 and UQCRH joining subsequently. The exact order of these events is yet to be determined[87]. As mentioned above, the initial phases of complex III_2 assembly are aided by the assembly factors UQCC1, UQCC2 and UQCC3 (REFS[37,38]). Then, the ISP, stabilized by and loaded with the Fe–S cluster by the chaperone protein MZM1L (MZM1-like protein, also known as LYRM7)[88], is inserted in the membrane via the translocase BCS1L[89–91]. ISP insertion is accompanied by concomitant insertion of UQCR10 and UQCR11 (REF.[92]). Lastly, in mammalian mitochondria, a different assembly factor, TTC19 (REFS[93,94]), participates in the clearance of the cleaved amino terminus of the ISP, which undergoes proteolysis before the Rieske protein assembly into the complex. The amino-terminal fragment of ISP has been observed in several structures of the mature complex III_2 and has been assigned as subunit 9 (REF.[95]). However, the low quality of the data has led to inconclusive assignment of the density and resulted in the suggestion that one copy of subunit 9 is cleared by TTC19, while the other remains bound to complex III_2 (REFS[83,96]). The recent structures of the murine supercomplexes $CIII_2CIV$ and $CICIII_2$ have clarified that indeed only one copy of subunit 9 remains bound to complex III_2, thereby confirming this suggestion[97].

Recently, a small peptide (8 kDa) associated with the IMM and responsive to the activation of AMPK signalling, named 'BRAWNIN', has been described as a potential novel player in the assembly of complex III_2 in vertebrates. This connection to AMPK could be an important mechanism adapting the ETC assembly in response to metabolic cues. BRAWNIN was shown to physically interact with the core proteins, but so far its precise role is unknown[98]. Importantly, correctly assembled complex III_2 is required for the maturation of complex I and complex IV, pointing towards a functional crosstalk among the ETC complexes[34].

Assembly, structure and mechanism of complex IV. Complex IV accepts the electrons delivered by cytochrome *c* (thereby oxidizing it) to reduce oxygen to water and additionally transfers one proton to the IMS for each cytochrome *c* molecule[99] (resulting in the pumping of four protons per each functional cycle). In most crystal structures of isolated complex IV, it appears as a dimer. Each complex IV monomer contains 13 well-established subunits, of which the three membrane-embedded core subunits are mitochondrial DNA-encoded, while the others are encoded in the nuclear genome[100]. Subunit 1 (MT-CO1) contains the two *a*-type haems, *a* and a_3, and the copper centre Cu_B, which is used to reduce oxygen to water, while subunit 2 (MT-CO2) harbours the copper centre Cu_A, the primary acceptor of electrons from the soluble carrier cytochrome *c*. The third core subunit, MT-CO3, contains three tightly bound phospholipids that have been proposed to regulate oxygen uptake and transfer to the active site: the insertion of their hydrophobic tails prevents the hydration of the space between protein helices, thus constituting a diffusion path for the hydrophobic oxygen molecules[101] (FIG. 2). An additional, 14th subunit, NDUFA4, has been identified in the monomeric structure of complex IV (see also the subsection Role of NDUFA4) at a position that would prevent dimer formation[102]. This can explain why this subunit was not resolved in the previous dimeric structures, although, as discussed later, this subunit is not observed in all the deposited monomeric structures of complex IV.

Complex IV assembles into three subcomplexes, each containing one of the core subunits, which then associate into the mature complex (FIG. 3a). This process is aided by almost 50 assembly factors[100,103] (see TABLE 1). The first module is formed by MT-CO1, plus two supernumerary subunits, COX4 and COX5A. This process involves multiple regulatory factors. MT-CO1 expression is regulated post-transcriptionally, which involves COX24, TACO1 and LRPPRC. The assembly

AMPK signalling
A pathway of intracellular reactions starting from AMPK (AMP-activated kinase), a sensor of the ATP levels. The signalling cascade starting from AMPK thus responds to the energetic demands of the cell and it triggers a high variety of responses pertaining to metabolism, growth, autophagy and cell polarity.

Copper centre
Prosthetic group composed of copper ions. Among the electron transport chain components, complex IV has two such centres involved in electron transfer.

Box 3 | **Coupling mechanism of complex I**

Our understanding of the mechanism of action of complex I has recently made a substantial leap forward as result of the publication of structures of ovine enzymes under different redox conditions, including turnover (that is, during the catalytic cycle)[40]. The figure summarizes the proposed mechanism stemming from these structures, showing transmembrane helices (TMHs; shown as cylinders) and residues (coloured circles) that are key for catalysis. These key residues can be protonated from the cytoplasm through several possible pathways, including inter-subunit transfer (indicated by black arrows: solid arrows represent the most likely pathways, while dashed arrows represent putative optional pathways). The high resolution of the data (~2.5 Å) allowed experimental modelling of water molecules, which is essential for the detection of proton translocation pathways. Helix HL at the matrix side and the βH hairpin elements at the intermembrane space (IMS) side of the membrane arm help to coordinate the concerted action of antiporters (ND2, ND4 and ND5). Electrons are transferred from the electron donor NADH via the iron–sulfur clusters (Fe–S clusters) (blue arrows). The terminal Fe–S cluster, N2, donates the electrons to quinone. The negatively charged quinone (or charged residues nearby) initiates a cascade of conformational changes (red, double-headed arrows), propagating from the quinone-binding site (Q site) to the E-channel (at ND1, ND6 and ND4L). Two main states of the enzyme were observed: 'open', with the larger angle between the two arms and Q site disrupted, and thus open to the matrix at the interface of the two arms; and 'closed', with the smaller angle between the arms and a closed Q site, with only the narrow exit into the lipid bilayer still open. During the catalytic cycle the enzyme cycles between the two states, with the following implications. During quinone reduction, complex I closes, while it is in the open conformation during the rest of the catalytic cycle. Furthermore, closing is accompanied by ordering of the key loops around the Q site in ND1, ND3 and 49-kDa subunits, as well as the rotation of the key helix TMH3 of ND6 (J3 in the figure), losing its characteristic π-bulge (disruption of the helix). As a consequence, these conformational changes connect the Q site, the E-channel and the previously postulated, and now experimentally confirmed, hydrated central hydrophilic axis of the membrane domain. Therefore, the two protons needed for the full reduction of quinone are proposed to come via the central axis, from the Glu residues indicated as two red circles with thicker outlines on subunit ND4L in the vicinity of subunit ND2, thereby transducing the signal (charge) from the Q site to the antiporter subunits. The key missing link in the communication between redox reaction and proton pumping in complex I is thus revealed.

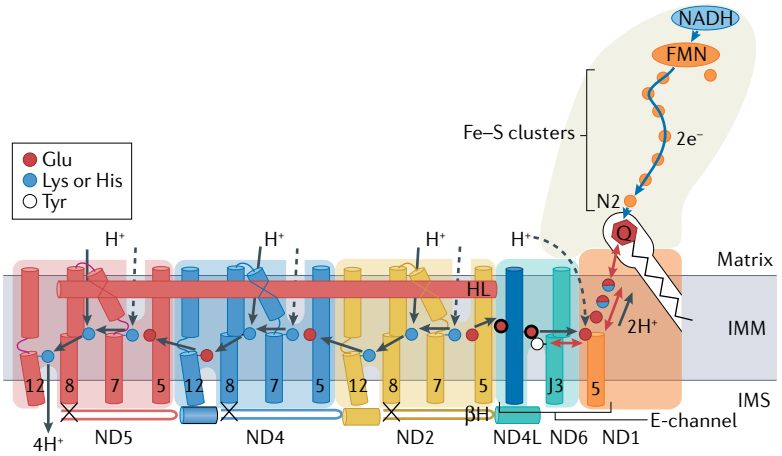

Additionally, the structure of the defined deactive state was reported, characterized by the striking relocation of TMH4 of ND6, so that the loop connecting TMH3 and TMH4 arrests the enzyme in the open state[40]. This differs from the previous description of the murine deactive state[155], which corresponds to the open state of active ovine complex I. The described active state of the murine enzyme[155] corresponds to the ovine closed state. One of the key differentiating features of the open state versus the closed state is the loop between TMH1 and TMH2 in ND3, which embraces the interface between the two arms. It is ordered only in the closed state, closing off the Q site from the mitochondrial matrix — a key part of the catalytic mechanism, forcing quinone protonation to occur via the E-channel. The recent high-resolution structure of complex I from the yeast *Yarrowia lipolytica* revealed fewer water molecules[39] due to lower resolution than in the ovine case but the general water distribution pattern is consistent with the ovine open state. In that study, it was proposed that quinone is protonated via a putative access path to the matrix in the 49-kDa subunit, which, however, would lack the electrostatic coupling and gating properties of the E-channel connection. So far, all *Y. lipolytica* complex I structures[39,60,216,217] do not show any changes around the π-bulge in ND6, suggesting that the entire repertoire of the catalytic intermediates in this species is yet to be captured and resolved by cryo-electron microscopy.

FMN, flavin mononucleotide; IMM, inner mitochondrial membrane. Figure adapted from REFS[49,215], Springer Nature Limited.

processes for haem *a* and Cu_B are instead aided by COX10 and COX15, and by COX11, COX17 and COX19, respectively. The assembly factors implicated in MT-CO1 formation include COX14, COA3, CMC1, CMC2, COA1, COA2, MDJ1, OMA1, OXA1, SURF1, SSC1 and MITRAC7, whereas association of COX4 and COX5A with MT-CO1 was linked to the assembly factor HIGD1A. The second module is composed of MT-CO2 and the nuclear DNA-encoded subunits COX6C, COX7B, COX7C, COX8A and COX5B. Its assembly is regulated by COX16, COX17, COX18, COX19, COX20, COX23, COA6, IMP1, IMP2, SCO1, SCO2, SOM1, TMEM177, MR-1S, MSS2, PNT1, PET100, PET111 and PET117. Finally, association of COX6A, COX6B and COX7A with the MT-CO3 module involves the assembly factors PET54, PET122, PET494 and HIGD2A[37,38,104]. Several additional factors are implicated in the assembly of complex IV, such as CEP89, COA5, COA7, COA8 and FASTKD2. Their mutations are associated with diseases, but their exact roles in the assembly of complex IV are elusive[37,103]. Interestingly, as complex III_2, also complex IV has been found to be required for the assembly of complex I, further contributing to the mutual control of the maturation of ETC complexes[105–107].

Mechanistically, at complex IV, four electrons are transferred one by one from the incoming cytochrome *c* molecules to an oxygen molecule via Cu_A, haem *a*, haem a_3 and Cu_B. This is coupled to a transport of four protons — required for oxygen reduction to water. These protons are transported from the matrix by proposed hydrated channels lined by protonatable residues, lysine (K) and aspartate (D), within the MT-CO1 subunit, which have been referred to as K and D pathways (as a reflection of the key residues forming the channels)[99]. In addition to these processes, each cycle of complex IV is coupled to the pumping of four additional

protons into the IMS. This occurs via the D pathway in all species, including the mammalian complex IV as shown recently[7] (and not via the previously discussed mammalian-specific H pathway, involving a hydrogen bond network that was initially proposed to function in proton pumping on the basis of the study of bovine mutants of complex IV (REF.[108])).

Assembly, structure and mechanism of complex V. Complex V exploits the proton gradient generated by complexes I, III_2 and IV to phosphorylate ADP and generate ATP[11] (FIG. 2a). ATP synthases can also function in the opposite direction, to generate proton-motive force via ATP hydrolysis (that is, functioning as ATPases)[109]. F-type ATP synthases produce ATP in the bacterial cytoplasm[110], mitochondrial matrix[43,44] and stroma of chloroplasts[111], V-type ATPases use ATP to pump protons into the vacuolar lumen[109] and A-type ATPases[42] can perform both functions and are found mainly in archaea[112].

Complex V features two main components: the F_o domain with the c-ring, which is membrane embedded and responsible for proton translocation, and the soluble F_1 domain — composed of three α-subunits and three β-subunits forming a globular assembly — which comprises the catalytic head responsible for the phosphorylation of ADP to ATP. The two are kept together by a central stalk (composed of γ, δ and ε subunits) and a peripheral stalk. The peripheral stalk is constituted by two subdomains: one soluble subdomain, connected to the F_1 domain and composed of subunits b, OSCP, F6 and d; and another, membrane-embedded subdomain, attached to the c-ring, and composed of subunits f, e, g, a, ATP8, DAPIT and 6.8PL (TABLE 1). The central stalk transmits the rotatory movement of the c-ring, upon proton translocation, to the F_1 domain, while the peripheral stalk prevents futile rotation of the αβ subunits of F_1. The mechanism of proton translocation coupled to ADP phosphorylation has been extensively studied and was recently visualized by means of high-resolution cryo-EM structures of various intact ATPases[42–44,109]. Briefly, the proton-motive force powers the rotation of the membrane-embedded c-ring. Passing through the two half-channels formed at the interface between subunit a and the c-ring, protons reach the conserved glutamate in the middle of the c-ring and subsequently leave on the opposite side of the membrane. Crucial for the unidirectional transfer of protons to and from the glutamate of the c-ring and to prevent leakage in the opposite direction is a conserved arginine residue (R159 in humans and other mammals) of subunit a, sitting at the convergence of the two oblique hydrophilic half-channels, essentially formed by subunit a, with contributions from subunits b, c and f[43,44]. The central stalk transmits the rotation to F_1, held in place by the peripheral stalk, driving the conformational changes in the αβ subunits that perform ADP phosphorylation.

The assembly of ATP synthase is a modular process (FIG. 3b), featuring the independent formation of five subcomplexes, aided by the assembly factors ATPAF1, ATPAF2, TMEM70, C7orf55 and TMEM242 (REFS[37,38,54]). They include the αβ hexamer, bound to the inhibitory factor IF1 (REF.[113]); the central stalk in the matrix; and the c-ring in the membrane. The peripheral stalk is assembled from the two, soluble and membrane-bound, subcomplexes. The αβ subunits assemble with the central stalk (intermediate 1 in FIG. 3b), followed by two possible pathways: either the c-ring (intermediate 2a) or the full peripheral stalk, with subunits f, g and e (intermediate 3a), attaches to the core soluble subunits. The last assembly step involves the addition of the two mitochondrial DNA-encoded subunits a and ATP8 (REF.[113]) and the module made of accessory subunits 6.8PL and DAPIT. Notably, a recent study on human cells depleted of specific ATP synthase subunits revealed the existence of different intermediates, in between intermediate 1 and the full ATP synthase[114]. In addition to the previously described intermediate 3a (FIG. 3b), two further possible pathways have been described: in pathway 4, subunits b, g and e attach to subunit f, then they attach to intermediate 2a with OSCP and subunit F6, and finally the peripheral stalk is completed with subunit d. Finally, pathway 2 was further elaborated, describing the sequential addition of subunits g and e (intermediate 2c) and then subunit f (intermediate 5) after the OSCP module (intermediate 2b). Because these pathways were inferred from cellular models lacking specific subunits, it is currently unknown whether any of these pathways are more physiologically relevant, or whether they might be linked to different environmental conditions.

In addition to reconciling the exact pathways of ATP synthase assembly, further studies are required to elucidate the specific assembly pathway of the enzyme's dimer — the functional oligomeric state of ATP synthase — which was shown to be required for the formation of mitochondrial cristae[115]. The available data suggest that subunits 6.8PL[44] and DAPIT[113] and the inhibitory factor IF1 (REFS[116,117]) are important for the dimerization[114]. Moreover, it is worth mentioning that ATP synthase has been found to have a role in cell death — in addition to the well-known role of cytochrome *c* in the apoptotic pathway[118] — via the formation of the permeability transition pore (PTP)[43]. Calcium[119] triggers and cyclophilin D[120] mediates PTP opening, but the mechanism by which they lead to cell death remained elusive. Cryo-EM studies on the visualization of the PTP formation by ATP synthase have just begun[43,121]. The mechanisms of PTP regulation and cristae formation by ATP synthase are discussed in Supplementary Box 1.

Higher-order assemblies of complexes

In addition to being assembled as single complexes in the IMM, the components of the ETC have long been demonstrated to gather into higher-order structures named 'supercomplexes', which can be preserved upon extraction from mitochondria with the mild detergent digitonin[31]. From mammalian mitochondria, cryo-EM structures of $CICIII_2CIV$ (REFS[24,27,122–124]) (also known as the respirasome; FIG. 3c) and $CICIII_2$ (REFS[23,122]) have been reported, in addition to the putative megacomplex $CI_2CIII_2CIV_2$ (REF.[26]), although the low resolution of the megacomplex structure poses questions about the

c-ring
Membrane-embedded domain of ATP synthase formed by multiple copies of subunit c, arranged in the shape of a ring. The number of copies differs across species, thereby changing the diameter of the ring: mammalian ATP synthase has eight copies.

IF1
Inhibitory factor 1 (IF1) of ATP synthase involved in the prevention of ATP hydrolysis due to reverse functioning of the enzyme.

Mitochondrial cristae
The ultrastructure of the inner mitochondrial membrane, characterized by deep invaginations, increasing the overall surface of the inner mitochondrial membrane. It is guided by the arrangement of dimers of ATP synthase in rows that impose the membrane curvature.

Permeability transition pore
(PTP). Channel-like proteinaceous pore located in the inner mitochondrial membrane responsible for leakage of large molecules (up to 1.5 kDa) from the mitochondrial matrix.

Cyclophilin D
Mitochondrial peptidyl-prolyl *cis–trans* isomerase and a member of the cyclophilin family, a group of proteins able to bind the antifungal peptide cyclosporin A. Cyclophilins are involved in protein folding, signal transduction and the immune system. Although the precise role of cyclophilin D is not clear, it is known to interact with ATP synthase and mediate the opening of the permeability transition pore.

Substrate channelling
Metabolic phenomenon by which the reaction product of an enzyme is directly processed as a substrate by another enzyme without being exchanged with the external solution.

solidity of the claim. In addition, the mammalian structures of $CIII_2CIV$ have just been published[97], after the yeast structures of $CIII_2CIV_1$ and $CIII_2CIV_2$ (REFS[28–30]) and plant $CIII_2CIV$ (REF.[22]) had become available (FIG. 1a inset on the right and FIG. 4).

Several roles of the supercomplexes have been proposed, from regulators of reactive oxygen species (ROS) production[125–130] to regulators of the OXPHOS system efficiency, by modulating the turnover rates[32,97], and in particular as core players in putative substrate channelling[105,131,132]. However, the substrate channelling function of supercomplexes has recently been questioned by biochemical data[133], and no consensus has been reached so far on their involvement in protection against excessive ROS production. Further high-resolution structural data of supercomplexes in different catalytic states and studies on ROS production by various supercomplexes will help to reach a conclusion on these debates. Interestingly, the fraction of complexes found in supercomplexes greatly differs from one complex to the other: for example, while most of complex I is found in the respirasome and $CICIII_2$, most of complex IV is free, either in a monomer or in a dimer form[134]. Different supercomplex distributions have also been observed in different tissues[135,136]. While this has been suggested to reflect the response to different metabolic needs of these tissues and hence differences in utilization of mitochondrial respiration, it has been pointed out that technical differences in the preparations, such as the amount of digitonin used for solubilization, can lead to highly discrepant results[137]. Therefore, more solid evidence is required to precisely determine the tissue distribution of supercomplexes and the physiological relevance that such distribution implies. Other than protection against excessive ROS production and catalysis modulation, supercomplexes have been proposed to have a role in the regulation of the stability of the individual complexes, and several

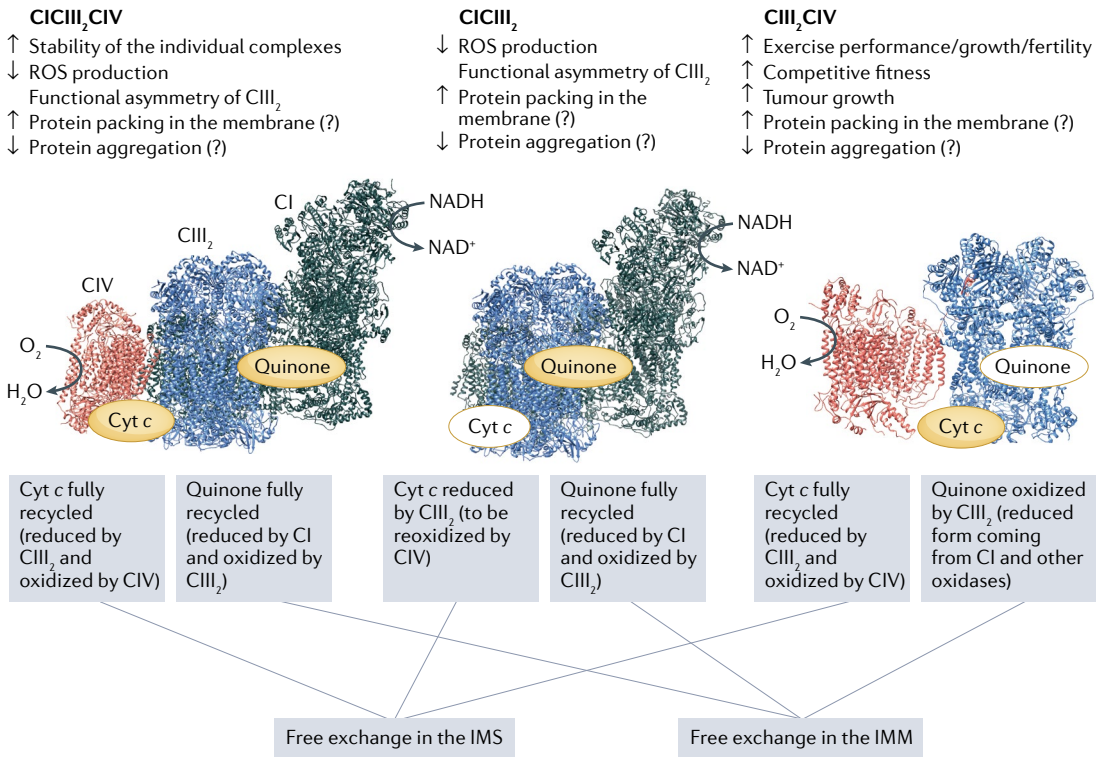

Fig. 4 | **Regulation of the electron transport chain by supercomplexes.** Outline of the existing supercomplexes (as atomic models, respirasome generated as in FIG. 3c, $CICIII_2$ Protein Data Bank (PDB) ID 6QBX and $CIII_2CIV$ PDB ID7O3C; CI refers to complex I, $CIII_2$ refers to complex III dimer and CIV refers to complex IV) and their functions, as described in the main text. Top: the main known or proposed physiological roles of each supercomplex are indicated. Question marks refer to the proposed but still debated roles. The models feature a scheme of the oxidoreduction reactions occurring within the supercomplexes ($NADH:NAD^+$ for complex I and $O_2:H_2O$ for complex IV). The exchange of the electron carriers (quinone and cytochrome *c* (cyt *c*)) is also indicated: when the carrier can be recycled within the supercomplex (meaning it is reduced by one complex and reoxidized by another), it is depicted as a yellow oval, while when only one of the two reactions happens, it is depicted as a white oval. The boxes below the models show that whether the carriers are fully recycled or not within the supercomplex, they can still be freely exchanged with the rest of the pool, in the inner mitochondrial membrane (IMM) for quinone and in the intermembrane space (IMS) for cytochrome *c*. This has profound physiological significance, because even though the efficiency of the reactions might be boosted by the spatial proximity of the complexes in supercomplexes, there are no segregate pools of carriers. Separate pools would mean that the maximal turnover rate is achieved within the supercomplexes, at the expense of a lower availability of carriers outside the supercomplexes and with no contribution from extra electron transport chain dehydrogenases. Free exchange, on the other hand, means that the carriers coming from a supercomplex component can donate the electrons, or be recycled, outside the supercomplex and vice versa. ROS, reactive oxygen species.

Endoplasmic reticulum stress
Aberrant condition characterized by the accumulation of unfolded proteins in the lumen of the endoplasmic reticulum

pieces of evidence have been accumulated recently that support this hypothesis.

Two models of supercomplex assembly were initially proposed: one according to which supercomplexes start to assemble from intermediates of the individual complexes[138] and one according to which they form only after the complexes are completed[139]. Recent publications suggest that the former might be the case. Human cell lines lacking the complex IV core subunits MT-CO1 and MT-CO2 were able to form supercomplexes with the remaining complex IV subunits[33], and pre-respirasomes were found with full complex III_2 and complex IV bound to an assembly intermediate of complex I lacking the N module[34]. These observations demonstrate that full complexes are not necessary for interactions in the context of supercomplexes. More precisely, it was further demonstrated that the P_D-a assembly module of complex I is sufficient to interact with complex III_2 and complex IV as a first step towards respirasome formation[140] (FIG. 3c). The deficiency of complex III_2 was also shown to affect the assembly of complexes I and IV (REF.[34]). In addition, the structure of the assembly intermediate of $CIII_2CIV$ features a full complex IV already bound to complex III_2 before subunits 10 and 11 and the ISP are fully ordered[97]. The formation of supercomplexes from assembly intermediates of the individual complexes thus suggests that supercomplexes play a crucial role in the regulation of cellular respiration by dictating the proportion of complexes in the isolated form even before they become catalytically active. Furthermore, as mentioned earlier, supercomplexes are the platform for the mutual regulation of the stability of complexes. It will therefore be of great interest to understand how the assembly of supercomplexes is regulated (see the next section).

Given the inconclusive evidence on protection against excessive ROS production and the ongoing debate on substrate channelling and despite the recent advances on the interplay of assembly between individual complexes and supercomplexes, their specific role in physiology and the contribution of their deregulated formation to disease remain largely elusive; recent reviews[137,141] summarize the findings in the field, especially related to widespread disorders such as heart failure, Alzheimer disease and Parkinson disease. The overall conclusion is that the current evidence for the physiological impact of supercomplex assembly is scarce and requires further investigation. Aside from biochemical investigation, the current state of cryo-EM would allow the study of supercomplex composition from samples obtained from humans, thereby allowing elucidation of their role in physiology, and in particular their connection to disease. In the next two sections, we review the latest findings on supercomplex assembly and function, highlighting the still debated issues in the field of respiratory supercomplexes.

Regulation of supercomplex assembly

Although this area of research is relatively nascent, we do have some data on how supercomplexes are formed. In particular, several factors — supercomplex assembly factor 1 (SCAF1), HIG and NDUFA4 — have been linked to these processes.

Role of SCAF1. A crucial supercomplex assembly factor is SCAF1, also known as COX7A2L, due to its homology to the complex IV subunit COX7A, or as COX7A-related polypeptide (COX7RP). SCAF1 is specifically required for the assembly of supercomplex $CIII_2CIV$ (REF.[135]) and has been found to be overexpressed in multiple cancer types, such as liver[129], breast and endometrial[130] carcinomas. Its deficiency has been linked to impaired exercise performance[105,142], body growth and fertility[143] as well as higher fat accumulation[142,143] and lower blood glucose levels[144] in animal models (FIG. 4). Interestingly, SCAF1 was recently found to be regulated by the endoplasmic reticulum stress sensor PERK as a result of glucose starvation[145]. Taken together, these observations specifically point towards the importance of SCAF1 in metabolism and more broadly exemplify the intricacy of the regulation of ETC function, which goes far beyond the simple activity of the individual complexes. The mechanism of SCAF1-mediated $CIII_2CIV$ assembly has also been investigated biochemically, showing that SCAF1 binds to an assembly intermediate of complex III_2, thus serving as a 'docking station' for complex IV (REFS[146,147]). Interestingly, the mammalian $CIII_2CIV$ structures revealed that this happens via the insertion of the amino terminus of SCAF1 into the cavity formed by the core 1 and core 2 subunits on the matrix side, while the carboxy terminus was found in complex IV in the position of subunit COX7A, as expected because SCAF1 is homologous to it. Thus, it appears that SCAF1 serves as a 'hook' to keep complex III_2 and complex IV together: it binds to complex III_2 and recruits complex IV before the assembly of complex III_2 is completed and keeps the supercomplex together in its mature form, thereby serving as a bona fide subunit, not only as an assembly factor. This is another piece of evidence in support of the intertwined assembly of single complexes and supercomplexes (FIG. 3c). One important remaining question concerns the possible role of SCAF1 in the assembly of the respirasome. On the one hand, complex III_2 and complex IV are components of the respirasome and SCAF1 has been biochemically, but not structurally, detected in a fraction of the respirasome[135,148]. On the other hand, it has been shown that although SCAF1 is necessary and sufficient for the formation of $CIII_2CIV$, it is apparently not required for the formation of the respirasome, which is recurrently observed in different *Scaf1*-knockout models[105,143,148]. In addition, C57BL/6 mice, harbouring a shorter version of SCAF1, are unable to form $CIII_2CIV$, but have been shown to feature the respirasome[149]. Furthermore, the structure of complex IV within the kidney-derived respirasome was shown to contain COX7A isoform COX7A2, and not SCAF1 (REF.[102]), and our results consistently show that complex IV from the heart respirasome harbours the muscle-specific isoform COX7A1 (REF.[97]). It has recently been proposed that SCAF1 would be required for the formation of both $CIII_2CIV$ and the tight conformation of $CICIII_2CIV$ (REF.[105]), but the lack of supporting structural evidence and the contrasting results (see Supplementary note for a potential explanation of the discrepancy) call for further investigations.

Hypoxia-inducible factor 1
Transcription factor primarily involved in the cellular response to hypoxia.

The recent structures of mammalian supercomplexes suggest that SCAF1 is not required for the assembly of the respirasome[97].

Role of HIGD and Rcf2. Another assembly factor involved in the biogenesis of supercomplexes is hypoxia-inducible gene domain (HIGD), which is induced by hypoxia-inducible factor 1 (HIF1) in response to changes in oxygen levels[150]; its role in the regulation of the ETC was recently reviewed[151], so here we briefly highlight the relevant information. In a seminal publication, HIGD1A was shown to be involved in the late stages of complex III_2 biogenesis, in assembly into supercomplexes and, to a lesser extent, in the maturation of complex IV (REF.[152]), to which it was shown to bind[100]. Complex IV maturation, in particular the formation of the MT-CO3 module, is more significantly controlled by the HIGD paralogue HIGD2A[153], which has also been observed to transiently interact with supercomplexes[152,153]. The association of HIGD1A and HIGD2A with supercomplexes is another piece of evidence in favour of crosstalk between the maturation of individual ETC complexes and of the supercomplexes. These factors have never been observed in structures, although, interestingly, the yeast member of the Hig1 family Rcf2 has recently been resolved as a constituent subunit of supercomplex $CIII_2CIV$ harbouring the hypoxic-specific isoform of supernumerary complex IV component COX5B[30]. Structures of mammalian $CIII_2CIV$ in normoxic versus hypoxic conditions, which are currently unavailable, would help shed light on a potential structural role for HIGD in supercomplexes and potential regulation of supercomplex assembly by hypoxia.

Role of NDUFA4. Similarly to HIGD, the role of the assembly factor NDUFA4 as an ETC component is still an enigma. Initially proposed as a subunit of complex I (REF.[154]), it has never been observed in the numerous currently available high-resolution structures of complex I, neither in the isolated form[40,155] nor within supercomplexes[24–26], extracted from membranes using the mild detergent digitonin (which should preserve interactions with more loosely attached subunits, which would otherwise be lost in presence of harsher detergents). On the other hand, although never observed in structures of isolated complex IV or complex IV dimer (CIV_2), NDUFA4 has been biochemically assigned as its 14th subunit[156]. Furthermore, its mutation has been linked to impaired complex IV, but not complex I, function[157], and it has recently been observed in the cryo-EM complex IV structure from the human respirasome[102]. The density of this subunit in this structure is weaker than in the rest of the complex and also a very weak and discontinuous density can be observed in the same position in the ovine tight respirasome[24], suggesting that this subunit is loosely attached. The position of NDUFA4 in the human complex IV structure argues against its possible role as a bridge between complex I and complex IV in the respirasome as it is not found at the interface of these complexes. These results suggest that NDUFA4 is indeed a structural subunit of complex IV, but given that it has been observed only in structures obtained by extraction and purification in the mild detergent digitonin, pointing towards a labile interaction with the rest of the complex, further work is required to fully elucidate its role in the function of the ETC.

Suggested functions of supercomplexes

As according to native polyacrylamide gel electrophoresis, cryo-EM and other data supercomplexes are widely present in mitochondria, from yeast to mammals and plants, it is tempting to speculate that they should have some functional significance. Here we outline the reported functions of supercomplexes and discuss the areas of debate.

Functional regulation of the activity of individual complexes via supercomplexes. The mutual regulation between assembly of single complexes and supercomplexes discussed earlier implies that formation of supercomplexes regulates the activity of the single complexes on two levels: first, by tuning their biogenesis, thus their existence in a catalytically active form in the IMM; and second, by modulating their catalytic efficiency thanks to the spatial proximity of substrate donor–acceptor sites. Several pieces of structural evidence support the function of supercomplexes as regulators of the activity of individual complexes. In the bovine respirasome structure[123], the soluble domain of the ISP subunit of complex III_2 proximal to the matrix arm of complex I is not visible, a sign of high mobility. By contrast, the same domain on the opposite, distal, protomer can be resolved, meaning that it is more rigid. As the movement of the ISP is required for complex III_2 function — enabling it to shuttle the electrons from cytochrome *b* to cytochrome c_1 via the Fe–S cluster — the study authors hypothesized that complex III_2 in the context of the respirasome does not function as a homodimer, as only the proximal ISP looks to be mobile. Further structural evidence consistent with this notion came from a more recent, higher-resolution structure of $CICIII_2$ (REF.[23]), in which two quinones were resolved at the haem b_H sites of complex III_2, but only one at the haem b_L site, suggesting, again, functional asymmetry of the two protomers. In addition, recent studies of the yeast supercomplex $CIII_2CIV$ revealed that the supercomplex provided higher quinol:O_2 oxidoreductase activity, while its specific disruption is responsible for reduced electron transfer via cytochrome *c*[32,158], resulting in lower cell fitness as compared with cells harbouring $CIII_2CIV$ (REF.[158]). Cryo-EM also showed that in this supercomplex, positively charged cytochrome *c* can 'roll' along a negatively charged patch on the surface of complex III_2 and complex IV, thereby diffusing within the supercomplex, while still in principle being free to exchange with the rest of the soluble pool[32]. These results have been confirmed in mammals[97], pointing towards a conserved function for supercomplex $CIII_2CIV$ across distant species. Additionally, animal models lacking the putative supercomplex assembly factor SCAF1 (see earlier) all demonstrate impaired metabolism, with phenotypes ranging from reduced body size to reduced fertility and exercise performance, pointing towards a crucial role

Metabolic flux control analysis
Mathematical description of a metabolic path where every enzymatic component is given a coefficient that describes the extent of its control over the pathway by correlating changes in the enzyme activity with changes in the flux rate.

Submitochondrial particles
Inverted vesicles of the inner mitochondrial membrane, obtained after disruption of the outer mitochondrial membrane via different mechanisms, such as osmotic shock, cycles of freezing and thawing or sonication.

Ischaemia–reperfusion injury
Pathological cellular response to reoxygenation of a tissue (reperfusion) after a period of hypoxia (ischaemia). At the molecular level, this phenomenon is characterized by an increase in the production of reactive oxygen species and activation of the caspase pathway, eventually leading to cell death.

Barth syndrome
A rare genetic disease, affecting mainly male individuals, characterized by neuromuscular deficiencies and associated with aberrant cardiolipin metabolism.

for supercomplexes (in this specific case $CIII_2CIV$) in mammalian metabolism.

Substrate channelling. Soon after the discovery of supercomplexes, metabolic flux control analysis performed on submitochondrial particles, or in mitochondria subject to freeze–thaw cycles to fracture membranes, showed that complex I and complex III_2 were equally controlling electron flux upon NADH oxidation[131]. These observations suggested that a pool of quinone sequestered within supercomplex $CICIII_2$ would be dedicated to direct transfer of electrons between the two complexes, without mixing with the rest of the membrane-embedded quinone. In other words, quinone (the substrate) would be shuttled (channelled) between the complexes and continuously recycled in a closed system (FIG. 4). This theory was supported by activity assays of the ETC components when their expression levels were modulated in cell lines and mouse-derived tissues[132]. However, extensive kinetic analysis of submitochondrial particles and mitochondrial membranes, including flux control analysis, reached opposite conclusions[159]. The involvement of supercomplexes in substrate channelling was further challenged by a subsequent study showing that externally added oxidase (AOX) was capable of oxidizing the reduced quinol coming from complex I in submitochondrial particles. This indicated that quinone is freely exchanged between complex I and its pool in the IMM, and is therefore not sequestered in the $CICIII_2$ or $CICIII_2CIV$ supercomplexes[133]. The biochemical experiments accompanying the $CICIII_2$ structures mentioned in the previous subsection also revealed that, in the purified supercomplex, complex I activity was limited by the exchange with the external quinone pool[23], further supporting the idea that substrate channelling does not happen between complex I and complex III_2. To date, the community is still divided on this topic. On the one hand, similar experiments with exogenous AOX were repeated (although on intact mitochondria instead of submitochondrial particles) and led to the suggestion that in presence of supercomplexes the available quinone is partitioned in two different pools[105]. On the other hand, in intact human cells, where most of complex I was shown to be found in supercomplexes, heterologously expressed AOX was able to rescue the drop in oxygen consumption caused by the complex III_2 inhibitor antimycin A, thereby arguing against the segregation of quinone between IMM-associated and supercomplex-associated pools[34]. In summary, although still supported by a few groups, the substrate channelling theory has been ruled out by most groups in the field on the basis of the ever-growing body of evidence against it.

Protection against excessive ROS generation. Respiratory supercomplexes have long been suggested to play a role in the protection against excessive production of ROS, oxygen-containing molecules characterized by the presence of unpaired electrons, which render them highly reactive. The first indication of this function comes from a study that showed a decrease in ROS levels generated by complex I — one of the main sources of mitochondrial ROS (along with complex III_2 (REF.[127])) — upon association of complex I with complex III_2 (REF.[25]) (FIG. 4). This was followed by a range of studies. For example, it has been shown that complex I is found mainly as an individual complex in astrocytes, whereas in neurons it is found mainly in supercomplexes, and this was correlated with different levels of ROS production[126], with astrocytes showing a significantly higher level of complex I-dependent ROS. A different study also showed that structural complex I impairment driven by ablation of the supernumerary subunit NDUFAB1 correlated with increased ROS production, decrease in the number of supercomplexes formed, accumulation of assembly intermediates of complex II and complex III_2 and eventually heart failure in mice. By contrast, overexpression of this protein led to a decrease of ROS production, increased number of supercomplexes and protection against ischaemia–reperfusion injury[128]. Despite these suggestive pieces of evidence, biochemical studies on isolated supercomplexes are required to directly link them to the reduction of excessive ROS production.

Additional proposed roles. In addition to the three putative functions described in the previous subsections, respiratory supercomplexes have been linked to other phenomena. For example, the disruption of mitochondrial cristae, the formation of which is involved in boosting respiration efficiency[160] and loss of which is observed during apoptosis[161], was found to cause dissociation of supercomplexes[162]. In turn, loss of supercomplexes was shown to be responsible for the altered turnover of the mitochondrial lipid cardiolipin — which regulates mitochondrial membrane properties, including assembly of protein complexes — in the rare X-linked human disorder Barth syndrome[163]. Cardiolipin is normally sequestered within the supercomplexes. However, in blood cells derived from patients with Barth syndrome, cardiolipin was released into the mitochondrial membrane and more readily degraded, and this was associated with disruption of supercomplexes in these cells[164]. On the basis of the correlation between mitochondrial membrane dynamics and supercomplex formation[162], it has also been proposed that they would allow tight packing of the ETC complexes in the IMM without protein aggregation and ensuring their homogeneous distribution in the membrane[159,165], but no further evidence has to date supported these hypotheses. Furthermore, the early proposal of supercomplexes existing as strings in the IMM[166] — essentially arranged as rows of a $CI_2CIII_2CIV_2$ megacomplex[26] — was confuted by subsequent in situ studies showing a random distribution of ETC supercomplexes in the membrane, unlike the ordered rows of ATP synthase, which are well established[122]. It has also been proposed that supercomplexes may control the stoichiometry of individual complexes. However, the facts that free complexes, especially complex IV, are observed in mitochondria and that different tissues have different composition of supercomplexes[31,122,134,167] argue against this theory. It is therefore clear that, despite the now widely accepted existence of respiratory supercomplexes and the growing body of evidence supporting their involvement in mitochondrial structure and

function, no consensus has been reached yet on their functional significance, and further research is needed. We envision that systematic analysis of the ETC at high resolution by cryo-electron tomography, now shown to be technically feasible, will pave the way towards better understanding of the importance of this higher-order structural assembly of respiratory complexes[168].

Conclusions and perspectives

In the past few years, a great deal of new information has advanced our understanding of the OXPHOS system, although several open questions remain.

Regarding the assembly of the different complexes, complex III_2 was found to be a key regulator of the formation of functional complex I and complex IV, as well as supercomplexes[34], thereby demonstrating an interplay among complexes, which eventually results in a mutual modulation of activity and impact on the overall turnover of the ETC. This role of complex III_2 also sheds new light on the function of supercomplexes, and challenges the initial view that supercomplexes form only after the assembly of functional individual complexes. New structural data also expanded our understanding of the role of ATP synthase in the formation and remodelling of mitochondrial cristae[115]. From the catalytic point of view, a recent milestone has been the elucidation of the coupling mechanism of complex I (REF.[40]), although the full details of the proton pumping mechanism remain to be established. In addition, again thanks to high-resolution cryo-EM structures, a detailed mechanism for proton translocation in ATPases has been described[43,44]. Moreover, the mammalian structures of $CIII_2CIV$ have described its unique SCAF1-mediated assembly, ruled out a role for SCAF1 in the assembly of the respirasome and confirmed the catalytic advantage of the supercomplexes over the isolated complexes, already observed in yeast.

Recently, a particularly large amount of work has been dedicated to understanding the assembly of supercomplexes and their roles in regulating the ETC. However, despite the growing availability of structural data on respiratory supercomplexes, much controversy remains in these areas. For example, the exact roles of assembly factors, such as HIG and NDUFA4, in supercomplex assembly have not yet been resolved and will require new high-resolution structural and biochemical data. Supercomplexes have also been ascribed to a number of functions, including protection against excessive ROS production, boosting the efficiency of the ETC by keeping the components in close proximity and sequestering a separate quinone pool, but no convincing data are currently available to support these hypotheses[134]. Future high-resolution structures of supercomplexes in different catalytic states, combined with functional studies on purified supercomplexes in solution, as well as in reconstituted liposomes, where the electrochemical gradient can be generated and controlled, will hopefully shed light on these aspects.

Published online: 07 October 2021

1. Nicholls, D. *Bioenergetics - 4th Edition* (Academic Press, 2013).
2. Green, D. E. & Tzagoloff, A. The mitochondrial electron transfer chain. *Arch. Biochem. Biophys.* **116**, 293–304 (1966).
3. Krebs, H. A. & Johnson, W. A. The role of citric acid in intermediate metabolism in animal tissues. *Enzymologia* **4**, 148–156 (1937).
4. Jones, A. J. Y., Blaza, J. N., Varghese, F. & Hirst, J. Respiratory complex I in Bos taurus and Paracoccus denitrificans pumps four protons across the membrane for every NADH oxidized. *J. Biol. Chem.* **292**, 4987–4995 (2017).
5. Mitchell, P. Possible molecular mechanisms of the protonmotive function of cytochrome systems. *J. Theor. Biol.* **62**, 327–367 (1976).
6. Trumpower, B. L. The protonmotive Q cycle. Energy transduction by coupling of proton translocation to electron transfer by the cytochrome bc1 complex. *J. Biol. Chem.* **265**, 11409–11412 (1990).
7. Maréchal, A. et al. A common coupling mechanism for A-type heme-copper oxidases from bacteria to mitochondria. *Proc. Natl Acad. Sci. USA* **117**, 9349–9355 (2020).
8. Rizwan, M., Rasheed, H. Al, & Tarjan, G. Succinate dehydrogenase complex: an updated review. *Arch. Pathol. Lab. Med.* **142**, 1564–1570 (2018).
9. Wang, Y. & Hekimi, S. Understanding ubiquinone. *Trends Cell Biol.* **26**, 367–378 (2016).
10. Alcázar-Fabra, M., Rodríguez-Sánchez, F., Trevisson, E. & Brea-Calvo, G. Primary coenzyme Q deficiencies: a literature review and online platform of clinical features to uncover genotype-phenotype correlations. *Free Radic. Biol. Med.* **167**, 141–180 (2021).
11. Mitchell, P. Coupling of phosphorylation to electron and hydrogen transfer by a chemi-osmotic type of mechanism. *Nature* **191**, 144–148 (1961).
12. Tang, J. X., Thompson, K., Taylor, R. W. & Oláhová, M. Mitochondrial OXPHOS biogenesis: co-regulation of protein synthesis, import, and assembly pathways. *Int. J. Mol. Sci.* **21**, 1–32 (2020).
13. Cogliati, S., Lorenzi, I., Rigoni, G., Caicci, F. & Soriano, M. E. Regulation of mitochondrial electron transport chain assembly. *J. Mol. Biol.* **430**, 4849–4873 (2018).
14. Priesnitz, C. & Becker, T. Pathways to balance mitochondrial translation and protein import. *Genes. Dev.* **32**, 1285–1296 (2018).
15. Cardenas-Rodriguez, M., Chatzi, A. & Tokatlidis, K. Iron–sulfur clusters: from metals through mitochondria biogenesis to disease. *J. Biol. Inorg. Chem.* **23**, 509–520 (2018).
16. Swenson, S. A. et al. From synthesis to utilization: the ins and outs of mitochondrial heme. *Cells* **9**, 579 (2020).
17. Pierron, D. et al. Cytochrome c oxidase: evolution of control via nuclear subunit addition. *Biochim. Biophys. Acta* **1817**, 590–597 (2012).
18. Xia, D. et al. Structural analysis of cytochrome bc1 complexes: implications to the mechanism of function. *Biochim. Biophys. Acta* **1827**, 1278–1294 (2013).
19. Stroud, D. A. et al. Accessory subunits are integral for assembly and function of human mitochondrial complex I. *Nature* **538**, 123–126 (2016).
20. Ghezzi, D. & Zeviani, M. Assembly factors of human mitochondrial respiratory chain complexes: physiology and pathophysiology. *Adv. Exp. Med. Biol.* **748**, 65–106 (2012).
21. Páleníková, P. et al. Duplexing complexome profiling with SILAC to study human respiratory chain assembly defects. *Biochim.Biophys. Acta Bioenerg.* **1862**, 148395 (2021).
22. Maldonado, M., Guo, F. & Letts, J. A. Atomic structures of respiratory complex III_2, complex IV, and supercomplex III_2-IV from vascular plants. *eLife* **10**, 1–34 (2021).
23. Letts, J. A., Fiedorczuk, K., Degliesposti, G., Skehel, M. & Sazanov, L. A. Structures of respiratory supercomplex I+III_2 reveal functional and conformational crosstalk. *Mol. Cell* **75**, 1131–1146.e6 (2019).
24. Letts, J. A., Fiedorczuk, K. & Sazanov, L. A. The architecture of respiratory supercomplexes. *Nature* **537**, 644–648 (2016).
25. Wu, M., Gu, J., Guo, R., Huang, Y. & Yang, M. Structure of mammalian respiratory supercomplex $I_1III_2IV_1$. *Cell* **167**, 1598–1609.e10 (2016).
26. Guo, R., Zong, S., Wu, M., Gu, J. & Yang, M. Architecture of human mitochondrial respiratory megacomplex $I_2III_2IV_2$. *Cell* **170**, 1247–1257 (2017).
27. Gu, J. et al. The architecture of the mammalian respirasome. *Nature* **537**, 639–643 (2016). **This, along with Letts et al. (2016), reported the first structure of the mammalian respirasome.**
28. Rathore, S. et al. Cryo-EM structure of the yeast respiratory supercomplex. *Nat. Struct. Mol. Biol.* **26**, 50–57 (2019).
29. Hartley, A. M. et al. Structure of yeast cytochrome c oxidase in a supercomplex with cytochrome bc^1. *Nat. Struct. Mol. Biol.* **26**, 78–83 (2019). **This, along with Rathore et al., reported the first structure of the mitochondrial yeast supercomplex $CIII_2CIV$.**
30. Hartley, A. M., Meunier, B., Pinotsis, N. & Maréchal, A. Rcf2 revealed in cryo-EM structures of hypoxic isoforms of mature mitochondrial III-IV supercomplexes. *Proc. Natl Acad. Sci. USA* **117**, 9329–9337 (2020).
31. Schägger, H. & Pfeiffer, K. Supercomplexes in the respiratory chains of yeast and mammalian mitochondria. *EMBO J.* **19**, 1777–1783 (2000). **First characterization of supercomplexes.**
32. Moe, A. et al. Cryo-EM structure and kinetics reveal electron transfer by 2D diffusion of cytochrome c in the yeast III-IV respiratory supercomplex. *Proc. Natl Acad. Sci. USA* **118**, e2021157118 (2021).
33. Lobo-Jarne, T. et al. Multiple pathways coordinate assembly of human mitochondrial complex IV and stabilization of respiratory supercomplexes. *EMBO J.* **39**, e103912 (2020).
34. Protasoni, M. et al. Respiratory supercomplexes act as a platform for complex III-mediated maturation of human mitochondrial complexes I and IV. *EMBO J.* **39**, e102817 (2020).
35. Fernandez-Vizarra, E. & Zeviani, M. Mitochondrial disorders of the OXPHOS system. *FEBS Lett.* **595**, 1062–1106 (2020).
36. Bratic, A. & Larsson, N. G. The role of mitochondria in aging. *J. Clin. Invest.* **123**, 951–957 (2013).
37. Mukherjee, S. & Ghosh, A. Molecular mechanism of mitochondrial respiratory chain assembly and its relation to mitochondrial diseases. *Mitochondrion* **53**, 1–20 (2020).
38. Signes, A. & Fernandez-Vizarra, E. Assembly of mammalian oxidative phosphorylation complexes I–V

and supercomplexes. *Essays Biochem.* **62**, 255–270 (2018).
39. Grba, D. N. & Hirst, J. Mitochondrial complex I structure reveals ordered water molecules for catalysis and proton translocation. *Nat. Struct. Mol. Biol.* **27**, 892–900 (2020).
40. Kampjut, D. & Sazanov, L. A. The coupling mechanism of mammalian respiratory complex I. *Science* **370**, eabc4209 (2020).
Structure-based description of the coupling mechanism of mammalian complex I.
41. Gutiérrez-Fernández, J. et al. Key role of quinone in the mechanism of respiratory complex I. *Nat. Commun.* **11**, 4135 (2020).
42. Zhou, L. & Sazanov, L. A. Structure and conformational plasticity of the intact Thermus thermophilus V/A-type ATPase. *Science* **365**, eaaw9144 (2019).
43. Pinke, G., Zhou, L. & Sazanov, L. A. Cryo-EM structure of the entire mammalian F-type ATP synthase. *Nat. Struct. Mol. Biol.* **27**, 1077–1085 (2020).
44. Spikes, T. E., Montgomery, M. G. & Walker, J. E. Structure of the dimeric ATP synthase from bovine mitochondria. *Proc. Natl Acad. Sci. USA* **117**, 23519–23526 (2020).
45. Fiedorczuk, K. et al. Atomic structure of the entire mammalian mitochondrial complex I. *Nature* **538**, 406–410 (2016).
46. Zhu, J., Vinothkumar, K. R. & Hirst, J. Structure of mammalian respiratory complex I. *Nature* **536**, 354–358 (2016).
47. Chomyn, A. et al. Six unidentified reading frames of human mitochondrial DNA encode components of the respiratory-chain NADH dehydrogenase. *Nature* **314**, 592–597 (1985).
48. Chomyn, A. et al. URF6, last unidentified reading frame of human mtDNA, codes for an NADH dehydrogenase subunit. *Science* **234**, 614–618 (1986).
49. Baradaran, R., Berrisford, J. M., Minhas, G. S. & Sazanov, L. A. Crystal structure of the entire respiratory complex I. *Nature* **494**, 443–448 (2013).
50. Formosa, L. E. et al. Dissecting the roles of mitochondrial complex I intermediate assembly complex factors in the biogenesis of complex I. *Cell Rep.* **31**, 107541 (2020).
51. Guerrero-Castillo, S. et al. The assembly pathway of mitochondrial respiratory chain complex I. *Cell Metab.* **25**, 128–139 (2017).
52. Formosa, L. E. et al. Optic atrophy–associated TMEM126A is an assembly factor for the ND4-module of mitochondrial complex I. *Proc. Natl Acad. Sci. USA* **118**, e2019665118 (2021).
53. Sánchez-Caballero, L. et al. TMEM70 functions in the assembly of complexes I and V. *Biochim. Biophys. Acta Bioenerg.* **1861**, 148202 (2020).
54. Carroll, J., He, J., Ding, S., Fearnley, I. M. & Walker, J. E. TMEM70 and TMEM242 help to assemble the rotor ring of human ATP synthase and interact with assembly factors for complex I. *Proc. Natl Acad. Sci. USA* **118**, e2100558118 (2021).
55. Pierrel, F. et al. Coa1 links the Mss51 post-translational function to Cox1 cofactor insertion in cytochrome c oxidase assembly. *EMBO J.* **26**, 4335–4346 (2007).
56. Leif, H., Sled, V. D., Ohnishi, T., Weiss, H. & Friedrich, T. Isolation and characterization of the proton-translocating NADH:ubiquinone oxidoreductase from Escherichia coli. *Eur. J. Biochem.* **230**, 538–548 (1995).
57. Sazanov, L. A. & Hinchliffe, P. Structure of the hydrophilic domain of respiratory complex I from Thermus thermophilus. *Science* **311**, 1430–1436 (2006).
58. Verkhovskaya, M. L., Belevich, N., Euro, L., Wikström, M. & Verkhovsky, M. I. Real-time electron transfer in respiratory complex I. *Proc. Natl Acad. Sci. USA* **105**, 3763–3767 (2008).
59. Berrisford, J. M. & Sazanov, L. A. Structural basis for the mechanism of respiratory complex I. *J. Biol. Chem.* **284**, 29773–29783 (2009).
60. Parey, K. et al. Cryo-EM structure of respiratory complex I at work. *eLife* **7**, e39213 (2018).
61. Bridges, H. R. et al. Structure of inhibitor-bound mammalian complex I. *Nat. Commun.* **11**, 1–11 (2020).
62. Verkhovskaya, M. & Bloch, D. A. Energy-converting respiratory complex I: on the way to the molecular mechanism of the proton pump. *Int. J. Biochem. Cell Biol.* **45**, 491–511 (2013).
63. Kaila, V. R. I. Long-range proton-coupled electron transfer in biological energy conversion: towards mechanistic understanding of respiratory complex I. *J. R. Soc. Interface* **15**, 20170916 (2018).
64. Iverson, T. M. Catalytic mechanisms of complex II enzymes: a structural perspective. *Biochim. Biophys. Acta Bioenerg.* **1827**, 648–657 (2013).
65. Sun, F. et al. Crystal structure of mitochondrial respiratory membrane protein complex II. *Cell* **121**, 1043–1057 (2005).
66. Moosavi, B., Berry, E. A., Zhu, X. L., Yang, W. C. & Yang, G. F. The assembly of succinate dehydrogenase: a key enzyme in bioenergetics. *Cell. Mol. Life Sci.* **76**, 4023–4042 (2019).
67. Huang, L. S. et al. 3-Nitropropionic acid is a suicide inhibitor of mitochondrial respiration that, upon oxidation by complex II, forms a covalent adduct with a catalytic base arginine in the active site of the enzyme. *J. Biol. Chem.* **281**, 5965–5972 (2006).
68. Scalliet, G. et al. Mutagenesis and functional studies with succinate dehydrogenase inhibitors in the wheat pathogen Mycosphaerella graminicola. *PLoS ONE* **7**, e35429 (2012).
69. Ruprecht, J. et al. Perturbation of the quinone-binding site of complex II alters the electronic properties of the proximal [3Fe-4S] iron-sulfur cluster. *J. Biol. Chem.* **286**, 12756–12765 (2011).
70. Yankovskaya, V. et al. Architecture of succinate dehydrogenase and reactive oxygen species generation. *Science* **299**, 700–704 (2003).
71. Oyedotun, K. S., Sit, C. S. & Lemire, B. D. The Saccharomyces cerevisiae succinate dehydrogenase does not require heme for ubiquinone reduction. *Biochim. Biophys. Acta Bioenerg.* **1767**, 1436–1445 (2007).
72. Blaut, M. et al. Fumarate reductase mutants of Escherichia coli that lack covalently bound flavin. *J. Biol. Chem.* **264**, 13599–13604 (1989).
73. Xia, D. et al. Crystal structure of the cytochrome bc1 complex from bovine heart mitochondria. *Science* **277**, 60–66 (1997).
74. Xia, D., Esser, L., Yu, L. & Yu, C. A. Structural basis for the mechanism of electron bifurcation at the quinol oxidation site of the cytochrome bc1 complex. *Photosynthesis Res.* **92**, 17–34 (2007).
75. Sarewicz, M. & Osyczka, A. Electronic connection between the quinone and cytochrome c redox pools and its role in regulation of mitochondrial electron transport and redox signaling. *Physiol. Rev.* **95**, 219–243 (2015).
76. Cooley, J. W., Roberts, A. G., Bowman, M. K., Kramer, D. M. & Daldal, F. The raised midpoint potential of the [2Fe2S] cluster of cytochrome bc_1 is mediated by both the Qo site occupants and the head domain position of the Fe-S protein subunit. *Biochemistry* **43**, 2217–2227 (2004).
77. Cooley, J. W., Ohnishi, T. & Daldal, F. Binding dynamics at the quinone reduction (Qi) site influence the equilibrium interactions of the iron sulfur protein and hydroquinone oxidation (Qo) site of the cytochrome bc1 complex. *Biochemistry* **44**, 55 (2005).
78. Cooley, J. W., Lee, D. W. & Daldal, F. Across membrane communication between the Q_o and Q_i active sites of cytochrome bc_1. *Biochemistry* **48**, 1888–1899 (2009).
79. Dikanov, S. A. et al. Identification of hydrogen bonds to the Rieske cluster through the weakly coupled nitrogens detected by electron spin echo envelope modulation spectroscopy. *J. Biol. Chem.* **281**, 27416–27425 (2006).
80. Sarewicz, M., Dutka, M., Pintscher, S. & Osyczka, A. Triplet state of the semiquinone-Rieske cluster as an intermediate of electronic bifurcation catalyzed by cytochrome bc_1. *Biochemistry* **52**, 6388–6395 (2013).
81. McCurley, J. P., Miki, T., Yu, L. & Yu, C. A. EPR characterization of the cytochrome b-c1 complex from Rhodobacter sphaeroides. *BBA Bioenerg.* **1020**, 176–186 (1990).
82. Sarewicz, M., Borek, A., Daldal, F., Froncisz, W. & Osyczka, A. Demonstration of short-lived complexes of cytochrome c with cytochrome bc1 by EPR spectroscopy: implications for the mechanism of interprotein electron transfer. *J. Biol. Chem.* **283**, 24826–24836 (2008).
83. Zong, S. et al. UQCRFS1N assembles mitochondrial respiratory complex-III into an asymmetric 21-subunit dimer. *Protein Cell* **9**, 586–591 (2018).
84. Ndi, M., Marin-Buera, L., Salvatori, R., Singh, A. P. & Ott, M. Biogenesis of the bc1 complex of the mitochondrial respiratory chain. *J. Mol. Biol.* **430**, 3892–3905 (2018).
85. Hildenbeutel, M. et al. Assembly factors monitor sequential hemylation of cytochrome b to regulate mitochondrial translation. *J. Cell Biol.* **205**, 511–524 (2014).
86. Gruschke, S. et al. The Cbp3-Cbp6 complex coordinates cytochrome b synthesis with bc1 complex assembly in yeast mitochondria. *J. Cell Biol.* **199**, 137–150 (2012).
87. Stephan, K. & Ott, M. Timing of dimerization of the bc1 complex during mitochondrial respiratory chain assembly. *Biochim. Biophys. Acta Bioenerg.* **1861**, 148177 (2020).
88. Sánchez, E. et al. LYRM7/MZM1L is a UQCRFS1 chaperone involved in the last steps of mitochondrial complex III assembly in human cells. *Biochim. Biophys. Acta* **1827**, 285–293 (2013).
89. Fernandez-Vizarra, E. et al. Impaired complex III assembly associated with BCS1L gene mutations in isolated mitochondrial encephalopathy. *Hum. Mol. Genet.* **16**, 1241–1252 (2007).
90. Wagener, N., Ackermann, M., Funes, S. & Neupert, W. A pathway of protein translocation in mitochondria mediated by the AAA-ATPase Bcs1. *Mol. Cell* **44**, 191–202 (2011).
91. Tang, W. K. et al. Structures of AAA protein translocase Bcs1 suggest translocation mechanism of a folded protein. *Nat. Struct. Mol. Biol.* **27**, 202–209 (2020).
92. Zara, V., Conte, L. & Trumpower, B. L. Evidence that the assembly of the yeast cytochrome bc1 complex involves the formation of a large core structure in the inner mitochondrial membrane. *FEBS J.* **276**, 1900–1914 (2009).
93. Bottani, E. et al. TTC19 plays a husbandry role on UQCRFS1 turnover in the biogenesis of mitochondrial respiratory complex III. *Mol. Cell* **67**, 96–105.e4 (2017).
94. Ghezzi, D. et al. Mutations in TTC19 cause mitochondrial complex III deficiency and neurological impairment in humans and flies. *Nat. Genet.* **43**, 259–263 (2011).
95. Berry, E. A., De Bari, H. & Huang, L. S. Unanswered questions about the structure of cytochrome bc1 complexes. *Biochim. Biophys. Acta* **1827**, 1258–1277 (2013).
96. Fernandez-Vizarra, E. & Zeviani, M. Mitochondrial complex III Rieske Fe-S protein processing and assembly. *Cell Cycle* **17**, 681–687 (2018).
97. Vercellino, I. & Sazanov, L. Structure and assembly of mammalian mitochondrial supercomplex $CIII_2CIV$. *Nature* https://doi.org/10.1038/s41586-021-03927-z (2021).
First structure of mammalian supercomplex $CIII_2CIV$.
98. Zhang, S. et al. Mitochondrial peptide BRAWNIN is essential for vertebrate respiratory complex III assembly. *Nat. Commun.* **11**, 1–16 (2020).
99. Yoshikawa, S. & Shimada, A. Reaction mechanism of cytochrome c oxidase. *Chem. Rev.* **115**, 1936–1989 (2015).
100. Timón-Gómez, A. et al. Mitochondrial cytochrome c oxidase biogenesis: recent developments. *Semin. Cell Dev. Biol.* **76**, 163–178 (2018).
101. Shinzawa-Itoh, K. et al. Structures and physiological roles of 13 integral lipids of bovine heart cytochrome c oxidase. *EMBO J.* **26**, 1713–1725 (2007).
102. Zong, S. et al. Structure of the intact 14-subunit human cytochrome c oxidase. *Cell Res.* **28**, 1026–1034 (2018).
103. Watson, S. A. & McStay, G. P. Functions of cytochrome c oxidase assembly factors. *Int. J. Mol. Sci.* **21**, 1–18 (2020).
104. Vidoni, S. et al. MR-1S interacts with PET100 and PET117 in module-based assembly of human cytochrome c oxidase. *Cell Rep.* **18**, 1727–1738 (2017).
105. Calvo, E. et al. Functional role of respiratory supercomplexes in mice: SCAF1 relevance and segmentation of the Qpool. *Sci. Adv.* **6**, eaba7509 (2020).
SCAF1-mediated modulation of supercomplexes assembly in mice.
106. Diaz, F., Fukui, H., Garcia, S. & Moraes, C. T. Cytochrome c oxidase is required for the assembly/stability of respiratory complex I in mouse fibroblasts. *Mol. Cell. Biol.* **26**, 4872–4881 (2006).
107. Čunátová, K. et al. Loss of COX4I1 leads to combined respiratory chain deficiency and impaired mitochondrial protein synthesis. *Cells* **10**, 369 (2021).
108. Yoshikawa, S., Muramoto, K. & Shinzawa-Itoh, K. Proton-pumping mechanism of cytochrome *c* oxidase. *Annu. Rev. Biophys.* **40**, 205–223 (2011).
109. Abbas, Y. M., Wu, D., Bueler, S. A., Robinson, C. V. & Rubinstein, J. L. Structure of V-ATPase from the mammalian brain. *Science* **367**, 1240–1246 (2020).
110. Morales-Rios, E. et al. Purification, characterization and crystallization of the F-ATPase from Paracoccus

denitrificans. *Open. Biol.* https://doi.org/10.1098/rsob.150119 (2015).
111. Hahn, A., Vonck, J., Mills, D. J., Meier, T. & Kühlbrandt, W. Structure, mechanism, and regulation of the chloroplast ATP synthase. *Science* **360**, eaat4318 (2018).
112. Grüber, G., Manimekalai, M. S. S., Mayer, F. & Müller, V. ATP synthases from archaea: the beauty of a molecular motor. *Biochim. Biophys. Acta* **1837**, 940–952 (2014).
113. He, J. et al. Assembly of the membrane domain of ATP synthase in human mitochondria. *Proc. Natl Acad. Sci. USA* **115**, 2988–2993 (2018).
114. He, J. et al. Assembly of the peripheral stalk of ATP synthase in human mitochondria. *Proc. Natl Acad. Sci. USA* **117**, 29602–29608 (2020).
115. Blum, T. B., Hahn, A., Meier, T., Davies, K. M. & Kühlbrandt, W. Dimers of mitochondrial ATP synthase induce membrane curvature and self-assemble into rows. *Proc. Natl Acad. Sci. USA* **116**, 4250–4255 (2019).
116. Cabezón, E., Arechaga, I., Butler, P. J. G. & Walker, J. E. Dimerization of bovine F1-ATPase by binding the inhibitor protein, IF1. *J. Biol. Chem.* **275**, 28353–28355 (2000).
117. Gu, J. et al. Cryo-EM structure of the mammalian ATP synthase tetramer bound with inhibitory protein IF1. *Science* **364**, 1068–1075 (2019).
118. Zou, H., Li, Y., Liu, X. & Wang, X. An APAf-1.cytochrome *c* multimeric complex is a functional apoptosome that activates procaspase-9. *J. Biol. Chem.* **274**, 11549–11556 (1999).
119. Haworth, R. A. & Hunter, D. R. The Ca^{2+}-induced membrane transition in mitochondria. II. Nature of the Ca^{2+} trigger site. *Arch. Biochem. Biophys.* **195**, 460–467 (1979).
120. Schinzel, A. C. et al. Cyclophilin D is a component of mitochondrial permeability transition and mediates neuronal cell death after focal cerebral ischemia. *Proc. Natl Acad. Sci. USA* **102**, 12005–12010 (2005).
121. Mnatsakanyan, N. et al. A mitochondrial megachannel resides in monomeric F1FO ATP synthase. *Nat. Commun.* **10**, 1–11 (2019).
122. Davies, K. M., Blum, T. B. & Kühlbrandt, W. Conserved in situ arrangement of complex I and III2 in mitochondrial respiratory chain supercomplexes of mammals, yeast, and plants. *Proc. Natl Acad. Sci. USA* **115**, 3024–3029 (2018).
In situ structural study of supercomplex arrangement from mitochondria of different species.
123. Sousa, J. S., Mills, D. J., Vonck, J. & Kühlbrandt, W. Functional asymmetry and electron flow in the bovine respirasome. *eLife* **5**, e21290 (2016).
124. Althoff, T., Mills, D. J., Popot, J.-L. & Kühlbrandt, W. Arrangement of electron transport chain components in bovine mitochondrial supercomplex $I_1III_2IV_1$. *EMBO J.* **30**, 4652–4664 (2011).
125. Maranzana, E., Barbero, G., Falasca, A. I., Lenaz, G. & Genova, M. L. Mitochondrial respiratory supercomplex association limits production of reactive oxygen species from complex I. *Antioxid. Redox Signal.* **19**, 1469–1480 (2013).
126. Lopez-Fabuel, I. et al. Complex I assembly into supercomplexes determines differential mitochondrial ROS production in neurons and astrocytes. *Proc. Natl Acad. Sci. USA* **113**, 13063–13068 (2016).
127. Quinlan, C. L., Perevoshchikova, I. V., Hey-Mogensen, M., Orr, A. L. & Brand, M. D. Sites of reactive oxygen species generation by mitochondria oxidizing different substrates. *Redox Biol.* **1**, 304–312 (2013).
128. Hou, T. et al. NDUFAB1 confers cardio-protection by enhancing mitochondrial bioenergetics through coordination of respiratory complex and supercomplex assembly. *Cell Res.* **29**, 754–766 (2019).
129. Wang, G., Popovic, B., Tao, J. & Jiang, A. Overexpression of COX7RP promotes tumor growth and metastasis by inducing ROS production in hepatocellular carcinoma cells. *Am. J. Cancer Res.* **10**, 1366–1383 (2020).
130. Ikeda, K. et al. Mitochondrial supercomplex assembly promotes breast and endometrial tumorigenesis by metabolic alterations and enhanced hypoxia tolerance. *Nat. Commun.* **10**, 1–15 (2019).
131. Blanchi, C., Genova, M. L., Castelli, G. P. & Lenaz, G. The mitochondrial respiratory chain is partially organized in a supercomplex assembly: hinetic evidence using flux control analysis. *J. Biol. Chem.* **279**, 36562–36569 (2004).
132. Lapuente-Brun, E. et al. Supercomplex assembly determines electron flux in the mitochondrial electron transport chain. *Science* **340**, 1567–1570 (2013).
Biochemical characterization of the respiratory supercomplexes, proposing the existence of separate quinone pools.
133. Fedor, J. G. & Hirst, J. Mitochondrial supercomplexes do not enhance catalysis by quinone channeling. *Cell Metab.* **28**, 525–531.e4 (2018).
Biochemical characterization of the respiratory supercomplexes, disproving the existence of separate quinone pools.
134. Lobo-Jarne, T. & Ugalde, C. Respiratory chain supercomplexes: structures, function and biogenesis. *Semin. Cell Dev. Biol.* **76**, 179–190 (2018).
135. Cogliati, S. et al. Mechanism of super-assembly of respiratory complexes III and IV. *Nature* **539**, 579–582 (2016).
136. Sun, D., Li, B., Qiu, R., Fang, H. & Lyu, J. Cell type-specific modulation of respiratory chain supercomplex organization. *Int. J. Mol. Sci.* **17**, 926 (2016).
137. Javadov, S., Jang, S., Chapa-Dubocq, X. R., Khuchua, Z. & Camara, A. K. Mitochondrial respiratory supercomplexes in mammalian cells: structural versus functional role. *J. Mol. Med.* **99**, 57–73 (2021).
138. Moreno-Lastres, D. et al. Mitochondrial complex I plays an essential role in human respirasome assembly. *Cell Metab.* **15**, 324–335 (2012).
139. Acín-Pérez, R., Fernández-Silva, P., Peleato, M. L., Pérez-Martos, A. & Enriquez, J. A. Respiratory active mitochondrial supercomplexes. *Mol. Cell* **32**, 529–539 (2008).
140. Fang, H. et al. A membrane arm of mitochondrial complex I sufficient to promote respirasome formation. *Cell Rep.* **35**, 108963 (2021).
141. Novack, G. V., Galeano, P., Castaño, E. M. & Morelli, L. Mitochondrial supercomplexes: physiological organization and dysregulation in age-related neurodegenerative disorders. *Front. Endocrinol.* **11**, 600 (2020).
142. Ikeda, K., Shiba, S., Horie-Inoue, K., Shimokata, K. & Inoue, S. A stabilizing factor for mitochondrial respiratory supercomplex assembly regulates energy metabolism in muscle. *Nat. Commun.* **4**, 1–9 (2013).
143. García-Poyatos, C. et al. Scaf1 promotes respiratory supercomplexes and metabolic efficiency in zebrafish. *EMBO Rep.* **21**, e50287 (2020).
144. Shiba, S. et al. Deficiency of COX7RP, a mitochondrial supercomplex assembly promoting factor, lowers blood glucose level in mice. *Sci. Rep.* **7**, 1–9 (2017).
145. Balsa, E. et al. ER and nutrient stress promote assembly of respiratory chain supercomplexes through the PERK-eIF2α Axis. *Mol. Cell* **74**, 877–890.e6 (2019).
146. Pérez-Pérez, R. et al. COX7A2L is a mitochondrial complex III binding protein that stabilizes the III2+IV supercomplex without affecting respirasome formation. *Cell Rep.* **16**, 2387–2398 (2016).
147. Lobo-Jarne, T. et al. Human COX7A2L regulates complex III biogenesis and promotes supercomplex organization remodeling without affecting mitochondrial bioenergetics. *Cell Rep.* **25**, 1786–1799.e4 (2018).
148. Fernández-Vizarra, E. et al. SILAC-based complexome profiling dissects the structural organization of the human respiratory supercomplexes in SCAFI KO cells. *Biochim. Biophys. Acta Bioenerg.* **1862**, 148414 (2021).
149. Mourier, A., Matic, S., Ruzzenente, B., Larsson, N. G. & Milenkovic, D. The respiratory chain supercomplex organization is independent of COX7A2L isoforms. *Cell Metab.* **20**, 1069–1075 (2014).
150. Ameri, K. et al. HIGD1A regulates oxygen consumption, ROS production, and AMPK activity during glucose deprivation to modulate cell survival and tumor growth. *Cell Rep.* **10**, 891–899 (2015).
151. Timón-Gómez, A., Bartley-Dier, E. L., Fontanesi, F. & Barrientos, A. HIGD-driven regulation of cytochrome c oxidase biogenesis and function. *Cells* **9**, 2620 (2020).
152. Timón-Gómez, A., Garlich, J., Stuart, R. A., Ugalde, C. & Barrientos, A. Distinct roles of mitochondrial HIGD1A and HIGD2A in respiratory complex and supercomplex biogenesis. *Cell Rep.* **31**, 107607 (2020).
153. Hock, D. H. et al. HIGD2A is required for assembly of the COX3 module of human mitochondrial complex IV. *Mol. Cell. Proteom.* **19**, 1145–1160 (2020).
154. Hayashi, T. et al. DJ-1 binds to mitochondrial complex I and maintains its activity. *Biochem. Biophys. Res. Commun.* **390**, 667–672 (2009).
155. Agip, A. N. A. et al. Cryo-EM structures of complex I from mouse heart mitochondria in two biochemically defined states. *Nat. Struct. Mol. Biol.* **25**, 548–556 (2018).
156. Balsa, E. et al. NDUFA4 is a subunit of complex IV of the mammalian electron transport chain. *Cell Metab.* **16**, 378–386 (2012).
157. Pitceathly, R. D. S. et al. NDUFA4 mutations underlie dysfunction of a cytochrome c oxidase subunit linked to human neurological disease. *Cell Rep.* **3**, 1795–1805 (2013).
158. Berndtsson, J. et al. Respiratory supercomplexes enhance electron transport by decreasing cytochrome *c* diffusion distance. *EMBO Rep.* **21**, e51015 (2020).
159. Blaza, J. N., Serreli, R., Jones, A. J. Y., Mohammed, K. & Hirst, J. Kinetic evidence against partitioning of the ubiquinone pool and the catalytic relevance of respiratory-chain supercomplexes. *Proc. Natl Acad. Sci. USA* **111**, 15735–15740 (2014).
160. Hackenbrock, C. R. Ultrastructural bases for metabolically linked mechanical activity in mitochondria. I. Reversible ultrastructural changes with change in metabolic steady state in isolated liver mitochondria. *J. Cell Biol.* **30**, 269–297 (1966).
161. Scorrano, L. et al. A distinct pathway remodels mitochondrial cristae and mobilizes cytochrome c during apoptosis. *Dev. Cell* **2**, 55–67 (2002).
162. Cogliati, S. et al. Mitochondrial cristae shape determines respiratory chain supercomplexes assembly and respiratory efficiency. *Cell* **155**, 160–171 (2013).
163. Barth, P. G. et al. An X-linked mitochondrial disease affecting cardiac muscle, skeletal muscle and neutrophil leucocytes. *J. Neurol. Sci.* **62**, 327–355 (1983).
164. Xu, Y. et al. Loss of protein association causes cardiolipin degradation in Barth syndrome. *Nat. Chem. Biol.* **12**, 641–647 (2016).
165. Hirst, J. Open questions: respiratory chain supercomplexes-why are they there and what do they do? *BMC Biol.* **16**, 111 (2018).
166. Dudkina, N. V., Kou□il, R., Peters, K., Braun, H. P. & Boekema, E. J. Structure and function of mitochondrial supercomplexes. *Biochim. Biophys. Acta Bioenerg.* **1797**, 664–670 (2010).
167. Chaban, Y., Boekema, E. J. & Dudkina, N. V. Structures of mitochondrial oxidative phosphorylation supercomplexes and mechanisms for their stabilisation. *Biochim. Biophys. Acta Bioenerg.* **1837**, 418–426 (2014).
168. Bouvette, J. et al. Beam image-shift accelerated data acquisition for near-atomic resolution single-particle cryo-electron tomography. *Nat. Commun.* **12**, 1957 (2021).
169. Yang, G. et al. Atp23p and Atp10p coordinate to regulate the assembly of yeast mitochondrial ATP synthase. *FASEB J.* **35**, e21538 (2021).
170. De Grassi, A., Lanave, C. & Saccone, C. Evolution of ATP synthase subunit c and cytochrome c gene families in selected metazoan classes. *Gene* **371**, 224–233 (2006).
171. Küster, U., Bohnensack, R. & Kunz, W. Control of oxidative phosphorylation by the extramitochondrial ATP/ADP ratio. *BBA Bioenerg.* **440**, 391–402 (1976).
172. Meyrat, A. & von Ballmoos, C. ATP synthesis at physiological nucleotide concentrations. *Sci. Rep.* **9**, 1–10 (2019).
173. Williams, G. I. Respiratory enzymes in oxidative phosphorylation III. The steady state. *J. Biol. Chem.* **217**, 409–427 (1955).
174. Wikström, M. & Springett, R. Thermodynamic efficiency, reversibility, and degree of coupling in energy conservation by the mitochondrial respiratory chain. *Commun. Biol.* **3**, 1–9 (2020).
175. Nicholls, D. G. The physiological regulation of uncoupling proteins. *Biochim. Biophys. Acta Bioenerg.* **1757**, 459–466 (2006).
176. Wang, W. & Seale, P. Control of brown and beige fat development. *Nat. Rev. Mol. Cell Biol.* **17**, 691–702 (2016).
177. Kory, N. et al. MCART1/SLC25A51 is required for mitochondrial NAD transport. *Sci. Adv.* **6**, eabe5310 (2020).
178. Luongo, T. S. et al. SLC25A51 is a mammalian mitochondrial NAD^+ transporter. *Nature* **588**, 174–179 (2020).
179. Girardi, E. et al. Epistasis-driven identification of SLC25A51 as a regulator of human mitochondrial NAD import. *Nat. Commun.* **11**, 1–9 (2020).
180. Ouyang, Y., Bott, A. J. & Rutter, J. Maestro of the SereNADe: SLC25A51 orchestrates mitochondrial NAD^+. *Trends Biochem. Sci.* **46**, 348–350 (2021).

181. Davila, A. et al. Nicotinamide adenine dinucleotide is transported into mammalian mitochondria. *eLife* **7**, e33246 (2018).
182. Mills, E. L. et al. Accumulation of succinate controls activation of adipose tissue thermogenesis. *Nature* **560**, 102–106 (2018).
183. Darvey, I. G. What factors are responsible for the greater yield of ATP per carbon atom when fatty acids are completely oxidised to CO_2 and water compared with glucose? *Biochem. Mol. Biol. Educ.* **27**, 209–210 (1999).
184. Rabinowitz, J. D. & Enerbäck, S. Lactate: the ugly duckling of energy metabolism. *Nat. Metab.* **2**, 566–571 (2020).
185. Brand, M. D. The efficiency and plasticity of mitochondrial energy transduction. *Biochem. Soc. Trans.* **33**, 897–904 (2005).
186. Warburg, O. On the origin of cancer cells. *Science* **123**, 309–314 (1956).
187. DeBerardinis, R. J. & Chandel, N. S. We need to talk about the Warburg effect. *Nat. Metab.* **2**, 127–129 (2020).
188. Bennett, N. K. et al. Defining the ATPome reveals cross-optimization of metabolic pathways. *Nat. Commun.* **11**, 1–16 (2020).
189. Wilson, D. F., Rumsey, W. L., Green, T. J. & Vanderkooi, J. M. The oxygen dependence of mitochondrial oxidative phosphorylation measured by a new optical method for measuring oxygen concentration. *J. Biol. Chem.* **263**, 2712–2718 (1988).
190. Lee, P., Chandel, N. S. & Simon, M. C. Cellular adaptation to hypoxia through hypoxia inducible factors and beyond. *Nat. Rev. Mol. Cell Biol.* **21**, 268–283 (2020).
191. Gorman, G. S. et al. Mitochondrial diseases. *Nat. Rev. Dis. Primers* **2**, 16081 (2016).
192. McFarland, R. & Turnbull, D. M. Batteries not included: diagnosis and management of mitochondrial disease. *J. Intern. Med.* **265**, 210–228 (2009).
193. Smeitink, J. A., Zeviani, M., Turnbull, D. M. & Jacobs, H. T. Mitochondrial medicine: a metabolic perspective on the pathology of oxidative phosphorylation disorders. *Cell Metab.* **3**, 9–13 (2006).
194. Ghezzi, D. & Zeviani, M. Human diseases associated with defects in assembly of OXPHOS complexes. *Essays Biochem.* **62**, 271–286 (2018).
195. Frazier, A. E., Thorburn, D. R. & Compton, A. G. Mitochondrial energy generation disorders: genes, mechanisms, and clues to pathology. *J. Biol. Chem.* **294**, 5386–5395 (2019).
196. Vafai, S. B. & Mootha, V. K. Mitochondrial disorders as windows into an ancient organelle. *Nature* **491**, 374–383 (2012).
197. Schubert, M. B. & Vilarinho, L. Molecular basis of Leigh syndrome: a current look. *Orphanet J. Rare Dis.* **15**, 1–14 (2020).
198. El-Hattab, A. W., Adesina, A. M., Jones, J. & Scaglia, F. MELAS syndrome: clinical manifestations, pathogenesis, and treatment options. *Mol. Genet. Metab.* **116**, 4–12 (2015).
199. Finsterer, J. & Zarrouk-Mahjoub, S. Leber's hereditary optic neuropathy is multiorgan not mono-organ. *Clin. Ophthalmol.* **10**, 2187–2190 (2016).
200. Fiedorczuk, K. & Sazanov, L. A. Mammalian mitochondrial complex I structure and disease-causing mutations. *Trends Cell Biol.* **28**, 835–867 (2018).
201. Dalla Pozza, E. et al. Regulation of succinate dehydrogenase and role of succinate in cancer. *Semin. Cell Dev.Biol.* **98**, 4–14 (2020).
202. Moosavi, B., Zhu, X. L., Yang, W. C. & Yang, G. F. Molecular pathogenesis of tumorigenesis caused by succinate dehydrogenase defect. *Eur. J. Cell Biol.* **99**, 151057 (2020).
203. Ryan, D. G. et al. Coupling Krebs cycle metabolites to signalling in immunity and cancer. *Nat. Metab.* **1**, 16–33 (2019).
204. Tannahill, G. M. et al. Succinate is an inflammatory signal that induces IL-1β through HIF-1α. *Nature* **496**, 238–242 (2013).
205. Mills, E. L. et al. Succinate dehydrogenase supports metabolic repurposing of mitochondria to drive inflammatory macrophages. *Cell* **167**, 457–470 (2016).
206. Bonello, S. et al. Reactive oxygen species activate the HIF-1α promoter via a functional NFκB site. *Arterioscler. Thromb. Vasc. Biol.* **27**, 755–761 (2007).
207. Weinberg, S. E. et al. Mitochondrial complex III is essential for suppressive function of regulatory T cells. *Nature* **565**, 495–499 (2019).
208. Fazakerley, D. J. et al. Mitochondrial CoQ deficiency is a common driver of mitochondrial oxidants and insulin resistance. *eLife* **7**, e32111 (2018).
209. Alcázar-Fabra, M., Navas, P. & Brea-Calvo, G. Coenzyme Q biosynthesis and its role in the respiratory chain structure. *Biochim. Biophys. Acta.* **1857**, 1073–1078 (2016).
210. Desbats, M. A., Lunardi, G., Doimo, M., Trevisson, E. & Salviati, L. Genetic bases and clinical manifestations of coenzyme Q10 (CoQ10) deficiency. *J. Inherit. Metab. Dis.* **38**, 145–156 (2015).
211. Martínez-Reyes, I. et al. Mitochondrial ubiquinol oxidation is necessary for tumour growth. *Nature* **585**, 288–292 (2020).
212. Liu, X., Kim, C. N., Yang, J., Jemmerson, R. & Wang, X. Induction of apoptotic program in cell-free extracts: requirement for dATP and cytochrome c. *Cell* **86**, 147–157 (1996).
213. Li, P. et al. Cytochrome c and dATP-dependent formation of Apaf-1/caspase-9 complex initiates an apoptotic protease cascade. *Cell* **91**, 479–489 (1997).
214. Li, K. et al. Cytochrome c deficiency causes embryonic lethality and attenuates stress-induced apoptosis. *Cell* **101**, 389–399 (2000).
215. Sazanov, L. A. A giant molecular proton pump: structure and mechanism of respiratory complex I. *Nat. Rev. Mol. Cell Biol.* **16**, 375–388 (2015).
216. Wirth, C., Brandt, U., Hunte, C. & Zickermann, V. Structure and function of mitochondrial complex I. *Biochim. Biophys. Acta* **1857**, 902–914 (2016).
217. Parey, K. et al. High-resolution cryo-EM structures of respiratory complex I: mechanism, assembly, and disease. *Sci. Adv.* **5**, eaax9484 (2019).

Author contributions

I.V. researched data for the article and wrote the article. All authors contributed substantially to discussion of the content and reviewed and/or edited the manuscript before submission.

Competing interests

The authors declare no competing interests.

Peer review information

Nature Reviews Molecular Cell Biology thanks E. Fernandez-Vizarra, M. Zeviani and the other, anonymous, reviewer(s) for their contribution to the peer review of this work.

Publisher's note

Springer Nature remains neutral with regard to jurisdictional claims in published maps and institutional affiliations.

Supplementary information

The online version contains supplementary material available at https://doi.org/10.1038/s41580-021-00415-0.